Chapter 19
Applications of Anthropogenic Radionuclides as Tracers to Investigate Marine Environmental Processes

G.-H. Hong, T.F. Hamilton, M. Baskaran, and T.C. Kenna

Abstract Since the 1940, anthropogenic radionuclides have been intentionally and accidentally introduced into the environment through a number of activities including nuclear weapons development, production, and testing, and nuclear power generation. In the ensuing decades, a significant body of research has been conducted that not only addresses the fate and transport of the anthropogenic radionuclides in the marine environment but allows their application as tracers to better understand a variety of marine and oceanic processes. In many cases, the radionuclides are derived entirely from anthropogenic sources and the release histories are well constrained. These attributes, in conjunction with a range of different geochemical characteristics (e.g., half-life, particle affinity, etc.), make the anthropogenic radionuclides extremely useful tools. A number of long-lived and largely soluble radionuclides (e.g., ^{3}H, ^{14}C, ^{85}Kr, ^{90}Sr, ^{99}Tc, ^{125}Sb, ^{129}I, ^{134}Cs, ^{137}Cs) have been utilized for tracking movement of water parcels in horizontal and vertical directions in the sea, whereas more particle-reactive radionuclides (e.g., ^{54}Mn, ^{55}Fe, ^{103}Ru, ^{106}Ru, Pu isotopes) have been utilized for tracking the movement of particulate matter in the marine environment. In some cases, pairs of parent-daughter nuclides (e.g., ^{3}H-^{3}He, ^{90}Sr-^{90}Y and ^{241}Pu-^{241}Am) have been used to provide temporal constraints on processes such as the dynamics of particles in the water column and sediment deposition at the seafloor. Often information gained from anthropogenic radionuclides provides unique/complementary information to that gained from naturally occurring radionuclides or stable constituents, and leads to improved insight into natural marine processes.

G.-H. Hong (✉)
Korea Ocean Research and Development Institute, Ansan P.O.Box 29 Kyonggi 425–600, South Korea
e-mail: ghhong@kordi.re.kr

T.F. Hamilton
Center for Accelerator Mass Spectrometry, Lawrence Livermore National Laboratory, Livermore, CA 94551–0808, USA

M. Baskaran
Department of Geology, Wayne State University, Detroit, MI 48202, USA

T.C. Kenna
Lamont-Doherty Earth Observatory, Columbia University, Palisades, NY 10964, USA

19.1 Introduction

Sustained atmospheric nuclear testings and bomb explosions from 1945 to 1980 in the Equatorial Pacific (Bikini Atoll, Christmas Island, Enewetak Atoll, Johnson Atoll), northern temperate latitudes (Algeria, Japan, Kapustin Yar, Lop Nor, New Mexico, Nevada Test Site, Semipalantinsk, Totsk), polar-north (Nova Zemlya), Southern Hemisphere (Fangatufa Atoll, Malden Island, Maralinga/EMU Test ranges, Monte Bello Islands, Mururoa Atoll) contaminated the entire surface of the earth including the ocean with a suite of anthropogenic radionuclides (Hamilton 2004), ranging from short-lived to long-lived radionuclides (Table 19.1). The oceanic inventory of some selected fallout anthropogenic radionuclides is listed in Table 19.2. Other source terms including effluents from nuclear waste reprocessing plants, nuclear power plants and nuclear weapons production facilities, accidents and losses involving nuclear materials, the burn-up of nuclear powered satellites in the atmosphere have all contributed to the anthropogenic radionuclide contamination (Hong et al. 2004; Linsley et al. 2004). Notably, releases from European nuclear fuel reprocessing facilities (primarily from Sellafield, UK and La Hague, France) have been documented in

M. Baskaran (ed.), *Handbook of Environmental Isotope Geochemistry*, Advances in Isotope Geochemistry,
DOI 10.1007/978-3-642-10637-8_19,

Table 19.1 List of anthropogenic radionuclides produced and globally dispersed, with their half-lives, decay mode and K_d. (a) Atmospheric nuclear weapon testing and discharge from reprocessing plants. (b) Radionuclides released from nuclear power plants in the United States[1]

(a)

Radio-nuclide (UNSCEAR 2000)	Half-life (UNSCEAR 2000; Browne and Firestone 1986)	K_d[a]	Decay mode (Browne and Firestone 1986)	Daughter (Browne and Firestone 1986)	Dominant form in seawater Byrne (2002) and in the surface of the earth (Bruland 1983; Emsley 1989) (nuclear reactions for the production of radionuclides) (Hou and Roos 2008)
H-3	12.32 a	1×10^0	β	$_2$He-3 (stable)	H_2O (gas, liquid, solid), biogenic matter, also produced by the natural process (^{2}H(n, γ)^{3}H; ^{3}He(n, p)^{3}H; ^{6}Li(n, α)^{3}H)
C-14	5730 a	2×10^3	β	$_7$N-14 (stable)	Gas CO_2, liquid, H_2CO_3, HCO_3^-, CO_3^{2-}, organic matter, biogenic or nonbiogenic (Ca,Mg or other metal) CO_3, also produced by the natural process ^{14}N(n, p)^{14}C; ^{13}C(n, γ)^{14}C; ^{17}O(n, α)^{14}C
Mn-54	312.5 d	2×10^8	EC, γ	$_{24}$Cr-54 (stable)	Ion $Mn^{2+}$and $MnCl^+$, solid MnO_2, $MnCO_3$, earth's crustal material, manganese nodule in the bottom of the sea, ferromanganese oxides (Fe, Mn)Ox, biogenic matter. ($Cr^{53}(d, n)Mn^{54}$) (Kafalas and Irvine 1956)
Fe-55	2.74 a	2×10^8	EC	$_{25}$Mn-54 (n, γ), $_{25}$Mn-55 (stable)	$Fe(OH)_3$, organic complex, contained in the phytoplankton cell, earth's crustal material
Se-79	2.95×10^5 a (Bienvenu et al. 2007)	1×10^3	β	$_{35}$Br-79 (stable)	Se, Se^{2+}, SeO_4^{2-}, SeO_3^{2-}, $HSeO_3^-$, earth's crustal material (^{78}Se(n, γ)^{79}Se; ^{235}U(n, f)^{79}Se)
Kr-85	10.72 a	1×10^0	β	$_{37}$Rb-85 (stable)	Noble gas, also produced by the natural process
Sr-89	50.55 d	2×10^2	β	$_{39}$Y-91	Sr^{2+}, largely soluble in seawater, forms $SrSO_4$ (celestite) by Aacantharia (protozoa) in upper 400 m, earth's crustal material
Sr-90	28.6 a	2×10^2	β	$_{39}$Y-90 (2.67 d) to $_{40}$Zr-90 (stable)	^{88}Sr(n, γ)^{89}Sr, (^{235}U(n, f)^{89}Sr; ^{88}Sr(n, γ)^{89}Sr, ^{235}U(n, f)^{90}Sr)
Y-91	58.51 d	7×10^6	β	$_{40}$Zr-91 (stable)	YCO_3^+, YOH^{2+}, Y^{3+}, particle reactive, earth's crustal material
Zr-93	1.53×10^6 a	7×10^6	β	$_{41}$Nb-93	$Zr(OH)_4^o$, $Zr(OH)_5^-$, earth's crustal material
Zr-95	64.03 d	7×10^6	β, γ	$_{41}$Nb-95(34.97 d) to $_{42}$Mo-95 (stable)	
Tc-99	2.13×10^5 a	1×10^2	β	$_{44}$Ru-99 (stable)	TcO_4^-, earth's crustal material (^{235}U(n, f)^{99}Tc; ^{98}Mo(n, γ)^{99}Mo(β)^{99}Tc)
Ru-103	39.25 d	1×10^3	β, γ	$_{45}$Rh-106 (29.8 s) to $_{46}$Pd-106	Earth's crustal material
Sb-125	2.73 a	4×10^3	β, γ	$_{52}$Te-125 (stable)	$Sb(OH)_5^0$/$Sb(OH)_6^-$, Earth's crustal material
I-129	1.57×10^7 a	2×10^2	β, γ	$_{54}$Xe-129	IO_3^- , I^- Dissolved in the water, incorporated into the seaweeds, lichens, grass, bovine thyroids (^{129}Xe(n, p)^{129}I; ^{235}U(n, f)^{129}I; ^{127}I(2n, γ)^{129}I) (^{130}Te (n, γ) ^{131}Te (β^-) ^{131}I)
I-131	8.02 d	2×10^2	β, γ	$_{54}$Xe-131(sable)	
Cs-137	30.14 a	2×10^3	β, γ	$_{56}$Ba-137 (stable)	Cs^+, earth's crustal material (^{235}U(n, f)^{137}Cs)

(*continued*)

Table 19.1 (continued)

(a)

Radio-nuclide (UNSCEAR 2000)	Half-life (UNSCEAR 2000; Browne and Firestone 1986)	K_d[a]	Decay mode (Browne and Firestone 1986)	Daughter (Browne and Firestone 1986)	Dominant form in seawater Byrne (2002) and in the surface of the earth (Bruland 1983; Emsley 1989) (nuclear reactions for the production of radionuclides) (Hou and Roos 2008)
Ba-140	12.75 d	9×10^3	β, γ	$_{57}$La-140 (1.68 d) to $_{58}$Ce-140 (stable)	Ba^{2+} , $BaSO_4$, earth's crustal material
Ce-141	32.50 d	7×10^7	β, γ	$_{59}$Pr-141 (stable)	$CeCO_3^+$, Ce^{3+}, $CeCl^{2+}$, earth's crustal material
Ce-144	284.9 d	7×10^7	β, γ	$_{59}$Pr-144 (7.2 min) to $_{60}$Nd-144 (2.1×10^5 a) to $_{58}$Ce-140	
Sm-151	90 a	5×10^5	β	$_{63}$Eu-151(stable)	$SmCO_3^+$, Sm^{3+}, $SmSO_4^+$, earth's crustal material
Eu-155	4.96 a	2×10^6	β, γ	$_{64}$Gd-155	$EuCO_3^+$, Eu^{3+}, $EuOH^{2+}$, $Eu(CO_3)_2^-$, earth's crustal material
Np-237	2.144×10^6 a	1×10^3	α	$_{91}$Pa-233 (27.01 d)	Trace in uranium mine, $^{238}U(n, 2n)^{237}U \rightarrow ^{237}Np$; $^{235}U(n, \gamma)^{236}U(n, \gamma)^{237}U \rightarrow ^{237}Np$
Pu-238	87.74 a	1×10^5	α	$_{92}$U-234	Soluble Pu(V), particulate Pu(IV) $^{235}U(n, \gamma)^{236}U(n, \gamma)^{237}U(\beta^-)^{237}Np(n, \gamma)^{238}Np(\beta^-)^{238}Pu$, $^{238}U(n, 2n)^{237}U(\beta^-)^{237}Np(n, \gamma)^{238}Np(\beta^-)^{238}Pu$
Pu-239	24,100 a	1×10^5	α, γ	$_{92}$U-235	$^{238}U(n, \gamma)^{239}U(\beta^-)^{239}Np(\beta^-)^{239}Pu$
Pu-240	6560 a	1×10^5	α, γ	$_{92}$U-236 (2.32×10^7 a)	$^{238}U(n, \gamma)^{239}U(\beta^-)^{239}Np(\beta^-)^{239}Pu(n, \gamma)^{240}Pu$
Pu-241	14.4 a	1×10^5	β	$_{95}$Am-241 (432.75 a)	$^{238}U(n, \gamma)^{239}U(\beta^-)^{239}Np(\beta^-)^{239}Pu(n, \gamma)^{240}Pu(n, \gamma)^{241}Pu$
Am-241	432.75 a	2×10^6	α	^{237}Np	$^{241}Pu(\beta^-)^{241}Am$

(b)

Noble gases	^{41}Ar, ^{85}Kr, ^{85m}Kr, ^{87}Kr, ^{131m}Xe, ^{133}Xe, ^{133m}Xe, ^{138}Xe
Others	^{3}H, ^{24}Na, ^{51}Cr, ^{54}Mn, ^{55}Fe, ^{56}Mn, ^{57}Co, ^{58}Co, ^{59}Fe, ^{60}Co, ^{65}Zn, ^{89}Sr, ^{90}Sr, ^{92}Sr, ^{95}Nb, ^{95}Zr, ^{97}Nb, ^{97}Zr, ^{99}Mo, ^{99m}Tc, ^{103}Ru, ^{106}Ru, ^{110m}Ag, ^{113}Sn, ^{122}Sb, ^{124}Sb, ^{131}I, ^{132}I, ^{132}Te, ^{133}I, ^{134}Cs, ^{134}I, ^{135}I, ^{136}Cs, ^{137}Cs, ^{138}Cs, ^{139}Ba, ^{140}Ba, ^{140}Pa, ^{141}Ce, ^{143}Ce, ^{144}Ce, ^{187}W, ^{239}Np

[a]K_d (dimensionless) = [concentration per unit mass of particulate (kg/kg or Bq/g dry weight)]/[Concentration per unit mass of water (kg/kg or Bq/kg)]. Value in parenthesis indicate that data area insufficient to calculate K_ds and was chosen to be equal to the K_ds of periodically adjacent elements (IAEA 2004)

Scandinavian waters and the northern portions of the North Atlantic (Irish, North, Norwegian, Barents and Greenland Seas) (Gray et al. 1995; Lindahl et al. 2005). Chernobyl derived contamination has been documented in the Mediterranean Sea and elsewhere (e.g., Buesseler and Livingston 1996; Livingston and Povinec 2000; Noureddine et al. 2008; Papucci et al. 1996). Former nuclear weapons program facilities in Siberia (e.g., the Techa and the Tom tributaries of the River Ob, the River Yenisey, Mayak plant explosion in 1957, Karachi Lake in 1967 reported in Vakulovsky 2001) continues to release anthropogenic radionuclides to the Arctic Ocean (e.g., Cooper et al. 1999; Kenna and Sayles 2002). While there is no more direct deposition of fall-out to the ocean (ceased since early 1980), a secondary pathway for global fallout nuclides reaching the oceans, such as continental run-off, release of anthropogenic radionuclides from estuarine processes, and atmospheric deposition of continental dust of previously deposited debris, becomes important in some ocean regions.

The anthropogenic radionuclides are the ubiquitous global contaminants as some of them descended from the stratosphere and landed at sea (Tables 19.1 and 19.2). Therefore, they have received great attention from the radiological protection purposes in both the

Table 19.2 Oceanic inventory of fission products and transuranium elements originating from globally dispersed debris, and local and regional deposition from atmospheric nuclear tests, including estimates of regional fallout from Pacific Ocean tests sites and deposition from SNAP-9A decay corrected to 1 January 2000 (reproduced from Hamilton 2004 with some modification, used with permission)

Radio-nuclide	Arctic ocean		Atlantic Ocean		Indian Ocean		Pacific Ocean		Total Oceanic Inventory	
	PBq	Kg	PBq	Kg	PBq	Kg	PBq	Kg	PBq	Kg
^{3}H									8000[a]	22
^{14}C									130[a]	3.9
^{90}Sr	2.0	0.40	51	10	22	4	114	23	189	37
^{99}Tc	0.001	1.8	0.03	46	0.01	20	0.07	110	0.11	178
^{129}I	0.000005	0.72	0.0012	18	0.000050	7.7	0.003	43	0.0005	69
^{137}Cs	3.2	1.0	81	25	34	11	182	57	300	93
^{237}Np	0.0003	11.3	0.007	263	0.002	94	0.02	888	0.03	1,256
^{238}Pu	0.002	0.0032	0.13	0.2	0.11	0.17	0.50	0.78	0.73	1.16
^{239}Pu	0.054	23	1.4	591	0.58	250	4.5	2960	6.5	2820
^{240}Pu	0.036	4.2	0.90	106	0.38	45	4.0	477	5.4	632
$^{239+240}Pu$	0.090	28	2.3	697	0.96	295	8.6	2436	12	3,456
^{241}Pu	0.17	0.046	4.3	1.1	1.8	0.48	24	6.2	30	7.9
^{242}Pu	0.00001	0.091	0.0003	2.3	0.0002	1.0	0.003	22	0.004	26
^{241}Am	0.04	0.29	0.92	7.2	0.39	3.1	3.7	29	5.1	40

[a]Taken from Povinec et al. (2010)

terrestrial and marine environment for the past 60 years. As anthropogenic radionuclides are introduced into the sea, they behave almost identical to their stable counterpart (Pu does not have stable nuclide) chemical elements (Table 19.1). Moreover, changes in the level and distribution of specific radionuclides and isotopic ratios in the oceans through radioactive decay and/or transport dynamics provide internal clocks (tracers) of many oceanographic processes including fluxes and input history (e.g., Bowen et al. 1980). The utility of these anthropogenic radionuclides was immediately recognized by the marine science community to apply them to understand the natural marine processes. Often the natural radionuclides present in the earth surface were simultaneously utilized to understand marine biogeochemical processes. The dynamics of water mass movement, biological particle formation, sorption-desorption reactions and decomposition processes, settling rates of particulate matter through the water column, and ultimate deposition of radionuclides onto the seafloor in various ocean basins are of prime interest in ocean geochemistry. In this connection, Broecker (1974) observed that "During the International Geophysical Year (July 1957–December 1958) the atomic technology boom that occurred during the Second World War finally reached the seas. Since then, the field has seen spectacular growth. Great advances have been made in our understanding of the substances dissolved in the sea and buried in the sediments and their utilization as guides to the nature of both past and present processes within the sea."

The application of anthropogenic radionuclides has been, however, often limited by the techniques available for sampling and analysis. Earlier analytical methods of most anthropogenic radionuclides required relatively large volumes of seawater (approximately several 100 L), followed by preconcentration and subsequent radiochemical processing and measurements using analysis resulting from radioactive decay using alpha, beta, and gamma ray spectrometers and mass spectrometric atom counting. However, the developments in instrumentation and technology in sample collection, preconcentration, and analysis have reduced the sample size as well as the time involved in processing and measurement of samples for many radionuclides. Readers are advised to consult the sampling and analytical protocols, such as Baskaran et al. (2009), for the individual anthropogenic radionuclide concerned.

A large number of studies of anthropogenic radionuclides in the ocean have contributed either directly or indirectly to the knowledge on the rates, pathways of advection, and physical mixing of ocean water, quantification of marine particle sinking rate and fate in the ocean interior and burial processes in the sea

floor. Numerous studies have applied these man-made tracers to study processes such as velocities of ocean current systems and their mixing rates, particle cycling and transport, sediment accumulation and mixing rates, and pore waters dynamics as well as biological processes (see review articles in Livingston and Povinec 2002; Sholkovitz 1983 and references therein). Here we have collated previous researches that utilize anthropogenic radionuclides to understand processes of circulation and mixing of ocean water, and transport and fate of the particulate matter in the ocean. Application of anthropogenic radionuclides to tracing material transport in the atmosphere, soil, sedimentation dynamics in estuaries, and transuranics are also presented in Chaps. 25 (Matisoff and Whiting), 16 (Du et al.), and 20 (Ketterer et al.), respectively, in this volume.

19.2 Principles of Application

In most cases, the ocean input history of anthropogenic radionuclides is relatively well known; therefore a large number of radionuclides were utilized to trace their carrier phases in the sea as time markers. In particular, a large number of network stations were monitored around the globe by the former Environmental Measurements Laboratory, U.S. Department of Energy and ^{90}Sr fallout were measured over 30 years (from 1952 onwards). Using a constant ratio between ^{90}Sr and other nuclides (such as ^{137}Cs/^{90}Sr, ^{239,240}Pu/^{90}Sr, etc.) in the nuclear-weapons testing-derived fallout, the history of atmospheric fallout of most of anthropogenic radionuclides was documented. Upon reaching the surface of the earth's, each nuclide behaves similar to their stable counterpart chemical elements (except those of plutonium and technetium, as plutonium and ^{99}Tc have no corresponding stable isotopes). The anthropogenic radionuclide carrier phases in the sea are water (dissolved phase), dissolved organic matter, suspended particulate matter, bottom sediments, and biota. The carrier phase of each radionuclide is determined by the chemistry of prevailing redox and acid–base conditions in situ. Chemical forms of radionuclides influence their solubility, cell-membrane transport and bioavailability, adsorptive behavior onto particles, oceanic residence times, and volatility in the sea. In some cases, a pair or multiple anthropogenic radionuclides originated from a particular source could serve to trace the provenance of the carrier phase material. The daughter products of some of the anthropogenic radionuclides have different particle-affinity than that of their parents and the disequilibrium between the daughters and parents may be used to trace the dynamics of particle formation, sinking rates in the ocean interior and deposition rates on the seafloor. Numerical modeling techniques can be used to improve our understanding of many different environmental processes, and may apply to pollution control on a local, regional and/or planetary scale including climate change predictions. Anthropogenic radionuclides are playing an even important role in helping test the validity of these models by providing ground-truth measurement data on rates and fluxes of carrier phases such as air and water. These measurements are on the input history of radionuclides tracers and their evolution through space and time.

19.2.1 Isotopic Composition of Different Radionuclide Contaminant Sources

The transuranic composition and relative abundance of fission products produced in nuclear explosions are proportional to the duration and intensity of neutron irradiation as well as the isotopic composition of the initial material. More intense the neutron flux (e.g., high versus low burn-up fuels or high versus low explosive yield of an atomic weapon) will lead to a higher proportion of heavier isotopes of transuranics and higher yields of fission products in the irradiated material. For example, fallout debris derived from high yield weapons tests will have a higher ^{240}Pu/^{239}Pu ratio and contain more ^{137}Cs relative to fallout from a low yield weapons tests. Levels of contamination originating from the reprocessing facilities will differ based on the nature and burn-up characteristics of the fuel (e.g., low burn-up fuel from the production of weapons-grade plutonium or high burn-up fuel resulting from nuclear power generation).

Numerous studies have used the source specific signatures of nuclear contaminants to reconstruct radionuclide time histories and delineate inputs from multiple sources. Much of the available isotopic information documents the isotopic signatures of various sources as they are recorded in different environmental samples (e.g. soils, sediments, biota, ice and water).

Table 19.3 Activity ratios of selected pair of anthropogenic radionuclides useful for marine environmental applications (taken from Hong et al. 2004, used with permission). (a) Activity ratios of selected pair of global fallout radionuclides. (b) Activity and atom ratios of anthropogenic radionuclides originated from various sources other than global fallout. Activity ratios are given at the year 2000

(a)

Radionuclides	Activity ratio	Reference
$^{3}H/^{90}Sr$	299	Aarkrog (2003)
$^{14}C/^{90}Sr$	0.3424	Aarkrog (2003)
$^{137}Cs/^{90}Sr$	1.52	Aarkrog (2003)
$^{238}Pu/^{239+240}Pu$	0.030	Baskaran et al. (1995, 2000)[a]
$^{239}Pu/^{90}Sr$	0.0105	Aarkrog (2003)
$^{240}Pu/^{90}Sr$	0.007	Aarkrog (2003)
$^{241}Pu/^{90}Sr$	0.2283	Aarkrog (2003)[a]
$^{241}Pu/^{239+240}Pu$	13–14	
$^{240}Pu/^{239}Pu$	0.6672 (activity ratio)	Hirose et al. (2001)
$^{239+240}Pu/^{137}Cs$	0.182 (atom ratio)	Kelly et al. (1999); Kim et al. (2004)
	0.12 (activity ratio)	Baskaran et al. (1995)

(b)

Source	$^{240}Pu/^{239}Pu$ (atom ratio)	$^{238}Pu/^{239+240}Pu$ (activity ratio)	$^{241}Am/^{239+240}Pu$ (activity ratio)	$^{137}Cs/^{134}Cs$ (activity ratio)	$^{137}Cs/^{90}Sr$ (activity ratio)	$^{239+240}Pu/^{137}Cs$ (activity ratio)	$^{238}U/^{235}U$ (atom ratio)
Chernobyl	0.40 (Warneke et al. 2002)	0.5 (Hirose et al. 2001)		2 (Aoyama et al. 1991)	12.1 (Aoyama et al. (1991)		
Effluent from Selafield	0.242 (Lee et al. 2001)	0.27 ± 0.02 (Baskaran et al. 1995)					
dumped reactors in Kara Sea		0.25–0.46 (Baskaran et al. 1995)					
Coral rock and top soil (Mururoa Atoll) (1997)		0.54 ± 0.16 (Irlweck and Hrnecek 1999)	1.69 ± 0.51				
Loose coral rocks		30.7 ± 8.6 (Irlweck and Hrnecek 1999)	5.0 ± 1.2				
Reactor							
MAGNOX reactor (GCR)		0.23[b] (Warneke et al. 2002)					15–32 before burn up (Warneke et al. 2002)
Pressurized heavy water reactor (PHWR)		0.41[b] (Warneke et al. 2002)					
Advanced gas-cooled reactor (AGR)		0.57[b] (Warneke et al. 2002)					
Pressure tube boiling water reactor (RBMK)		0.67[b] (Warneke et al. 2002)					

Boiling water reactor (BWR)		0.40[b] (Warneke et al. 2002)		
Pressurized water reactor (PWR)		0.43[b] (Warneke et al. 2002)		
Natural uranium				137.88 (Warneke et al. 2002)
Weapon grade uranium				<0.1 (Warneke et al. 2002)
Depleted uranium				250–500 (Warneke et al. 2002)
Weapon production	0.01–0.07 Warneke et al. 2002)			
Ivy/Mike shot Eniwetok Island	0.36 (Koide et al. 1985)			
Rongelap atoll	0.276 (Muramatsu et al. 2001)		0.28	
Bikini atoll	0.306 (Muramatsu et al. 2001)		0.12	
Enewetak atoll (Runit Island)	0.065 (Muramatsu et al. 2001)		34.7	
Enewetak atoll (Aej Island)	0.254 (Muramatsu et al. 2001)		1.06	
Marshall Island	0.303 (Muramatsu et al. 2001)		0.20	
Semipalantinsk, Chenaya Guba, Nevada test sites soils	0.03–0.08 (Muramatsu et al. 2001)			
Nagasaki, Japna	0.037 (Yoshida and Muramatsu 2003)			
Mururoa and Fangataufa, sediments	0.035–0.05 (Chiappini et al. 1999)			

[a]Decay corrected to the year of 1 January 2000 using Aarkrog (1988) for the northern hemisphere
[b]After fuel burn-up

A list of useful activity and atom ratios of selected pairs of anthropogenic radionuclides in marine environmental applications are shown in Table 19.3.

19.2.2 Radioactive Fallout from Nuclear Weapons Tests

Atmospheric and aboveground testing of nuclear weapons is significant because it results in the injection of radioactive material into the stratosphere and troposphere; the subsequent deposition of this material on the planet's surface is termed fallout. Fallout can generally be divided into two types: global fallout and local (or close-in) fallout. Global fallout occurs when an explosion of sufficient yield occurs, and the debris is injected into the stratosphere. The deposition pattern of global fallout exhibits a latitudinal dependence with maxima at mid-latitudes and minima at the poles and equator. This is due to the fact that large volumes of air exit the stratosphere via the tropopause discontinuity in the mid-latitudes. Since interhemispheric-stratospheric exchange of materials occurs on longer time scales than materials exchanged between the stratosphere and troposphere, most global fallout is deposited within its hemisphere of origin (Perkins and Thomas 1980).

It is estimated that about 6,500, 4,300, and 40 TBq (4×10^{13} Bq) of ^{239}Pu, ^{240}Pu, and ^{237}Np, respectively have been released globally by the surface and atmospheric weapons tests conducted between 1945 and 1980 (Lindahl et al. 2005). Due to the long half-lives of these radionuclides, these values have not changed substantially. The estimates for ^{137}Cs reached a maximum during the mid to late 1960 of 460 PBq (4.6×10^{17} Bq). Due to its relatively short half-life, this value will have decreased to about 170 PBq by 2010. Of these total, approximately 76% was deposited in the northern hemisphere, nearly all being deposited between 0° N and 70°. Using a value of 55% of oceanic areal coverage, it is estimated that 2,500, 1,600, and 15 TBq and 71 PBq of ^{239}Pu, ^{240}Pu, ^{237}Np, and ^{137}Cs, respectively have been deposited to the marine areas of the Northern Hemisphere (Lindahl et al. 2005; UNSCEAR 2000).

While the initial pathway of fallout nuclides to the marine environment was direct deposition, a secondary pathway for global fallout nuclides reaching the oceans is continental run-off and related estuarine processes and tropospheric resuspension of previously deposited debris that may serve to modify the global fallout isotopic signatures (e.g., Linsalata et al. 1985; Shlokovitz and Mann 1987; Hamilton et al. 1996; see discussion below about the different geochemical behavior of the radionuclides of interest).

19.2.3 Discharges from the Nuclear Fuel Reprocessing Plant

A number of nuclear fuel reprocessing plants are located at the coast and they discharge radioactive wastes into the sea (Hu et al. 2010). The Sellafiled and La Hague in the northern Europe are of global significance in terms of ocean process tracers. The Sellafield Nuclear reprocessing plant has been discharging liquid radioactive wastes containing plutonium isotopes, ^{237}Np, and ^{137}Cs (with some amounts of ^{134}Cs) to the Irish Sea. It has been estimated that 610 and 9.5 TBq (1 TBq $= 10^{12}$ Bq) of ^{239,240}Pu and ^{237}Np, respectively and ~20 PBq (1 PBq $= 10^{15}$ Bq) of ^{137}Cs (decay corrected to 2010) have been released since the plant began operating in 1952 (Assinder 1999; Beasley et al. 1988; Gray et al. 1995; Kuwabara et al. 1996). The reported atom ratios of ^{240}Pu/^{239}Pu and ^{237}Np/^{239}Pu in discharges from Sellafield weighted over the operating period of the plant are 0.242 and 1.69, respectively. The La Hague Plant located in the west of Cherbourg, France began operating in 1966. Its radioactive waste discharge peaked in the late 1970 to early 1980. The cumulative discharge from La Hague between 1967 and 1995 was 33, 1,600, 654, 1.3 and 2.5 TBq of ^{60}Co, ^{90}Sr, ^{137}Cs, ^{238}Pu, $^{239+240}$Pu, respectively (Cundy et al. 2002). The 1997 sample of effluent showed a relatively high ^{240}Pu/^{239}Pu of 0.34 (Ketterer and Szechenyi 2008). La Hague also discharged ^{129}I as much as 1,640 kg for the period of 1975–1997 (Raisbeck and Yiou 1999).

19.2.4 Chernobyl Derived Contamination

It is estimated that the total activity of ^{239,240}Pu and ^{137}Cs released to the environment as a result of the accident at Chernobyl (April 1986) was 0.055 and 85 PBq (24 PBq in 2010), respectively. Kirchner

and Noack (1988) estimate that the $^{240}Pu/^{239}Pu$ and $^{237}Np/^{239}Pu$ atom composition in the reactor core at the time of the accident were 0.56 ± 0.16 and 0.023 ± 0.006, respectively. Although there are no published values for Chernobyl derived ^{237}Np, $^{240}Pu/^{239}Pu$ atom ratios of around 0.4 have been determined in soils near the facility (Krey et al. 1986; Muramatsu et al. 2000). Several studies of the Chernobyl accident have shown that the deposition pattern of radioactivity was highly variable over Europe and that the isotopic composition of this material varied throughout the period of the accident (Buesseler and Livingston 1996; Krey et al. 1986; Livingston et al. 1988). Chernobyl-derived ^{137}Cs was estimated to have added 5 and 3 PBq into the Baltic and Black Seas, respectively (Livingston and Povinec 2000) and 3 PBq in the Mediterranean Sea (Papucci et al. 1996).

19.3 Applications of Selected Anthropogenic Radionuclides

19.3.1 Tritium (^3H)

One of the most significant applications of anthropogenic radionuclides to climate studies up to the present is the utilization of the bomb tritium distribution in the North Atlantic (Fig. 19.1). With its presence in intermediate and deep waters, it directly confirmed that the deep water forms in the North Atlantic as postulated by the box model of global ocean conveyor-belt circulation (Broecker 1974). Before the era of nuclear weapons testing, the world's inventory of cosmic ray-produced tritium was estimated to be ~7 kg, however, by the time of the moratorium on widespread testing in 1963 an additional amount of the order of 100 kg had been introduced largely to the northern hemisphere. Both natural and anthropogenic tritium is rapidly transferred to the surface ocean as HTO ($^1H^3HO$) via direct precipitation and gas exchange. Tritium decays to ^3He with 12.43 years half-life. Bomb-produced tritium has considerable potential as a tracer for oceanic circulation and for the study of processes with time-scales of less than 100 years due to its short half-life. Tritium is normally reported in Tritium unit ($1\ TU = 1 \times 10^{-18}$ atoms of ^3H per atom of hydrogen or 1 tritium atom in 10^{18} hydrogen atoms; $1\ TU = 3.19\ pCi/L = 118\ Bq\ m^{-3}$). In subsurface waters, the ^3He thus formed cannot escape, so that the combined measurements of tritium and the in situ grown ^3He enables tritium$-^3He$ "dating", the age is the period since the parcel of water left the surface mixed layer (Roether et al. 1999)

The tritium/^3He age, $\tau_{He\text{-}3}$, is calculated using (19.1),

$$\tau_{He-3} = T_{1/2}/\ln 2 \times \ln(1 + [^3He_{-tri}]/[^3H]) \quad (19.1)$$

where $T_{1/2}$ is a half life of tritium (^3H) and $^3He_{-tri}$ is tritiogenic ^3He.

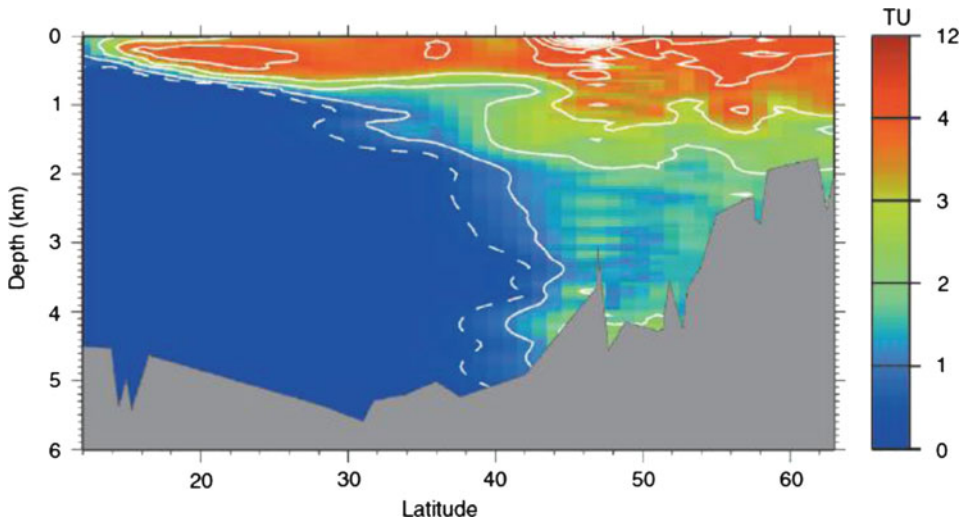

Fig. 19.1 A North Atlantic tritium meridional section in the Denmark Strait to the Central Sargasso Sea taken in the early 1980. The extensive penetration of bomb tritium in the Norwegian Sea (60°N) is clearly visible (Jenkins 2001, used with permission)

Due to radioactive decay, the bomb-produced tritium inventory has reduced from 113,000 PBq at 1963 to 8,000 PBq in 2010 or only about 4 times larger than the natural fallout level. The reprocessing plants-originated ^{3}H oceanic inventory is estimated to be 45 PBq in 2010 (Povinec et al. 2010). And after cessation of bomb-derived ^{3}H global fallout in the early 1980, the water circulation and mixing appears to influence ^{3}H distribution in the ocean more than the atmospheric input in the past.

19.3.2 Radiocarbon (^{14}C)

Radiocarbon is also produced naturally in the atmosphere by nuclear reaction of cosmic ray-produced neutrons with atmospheric nitrogen. The ^{14}C production rate of 2.2 atoms cm^{-2} s^{-1} is balanced by its disintegration by beta decay. During its mean lifetime of 8,200 years radiocarbon can penetrate the active carbon reservoirs through chemical reactions of carbonic acid formation and plant photosynthesis (Fig. 19.2). The production rate of ^{14}C has not been constant with time, and neither have the rates of processes that distribute ^{14}C among various reservoirs. In addition to these natural perturbations, the emission of CO_2 to the atmosphere by fossil fuel combustion has measurably reduced the atmospheric $^{14}C/^{12}C$ ratio. The large input of ^{14}C into the upper atmosphere resulting from nuclear weapon testing became measurable in 1954. At the time of the implementation of the test ban treaty in 1963, the number of nuclear-weapons-derived ^{14}C atoms in the atmosphere was roughly equal to the number of cosmogenic ^{14}C atoms. This excess ^{14}C has decreased to ~10% of the cosmogenic ^{14}C inventory as of the year 2000 (Broecker 2003). This decrease is mainly due to removal of ^{14}C by the exchange with ocean ΣCO_2 and terrestrial biospheric carbon and dilution by the addition of ^{14}C free fossil-fuel-derived CO_2 molecules to the atmosphere (Broecker 2003). And the current atmospheric and biotic mass activities of ^{14}C are close to levels observed prior to atmospheric nuclear weapons testing (Yim and Caron 2006).

As it is difficult to measure absolute ^{14}C concentrations, it is conventional to express ^{14}C determinations as the per mil difference between the specific activity of the sample and 0.95 times the activity of a standard carbon sample ($A_{NBS\ Std}$), with the 'modern' is defined as the year of 1950. Thus

$$\delta^{14}C = (A_{sample} - 0.95A_{NBS\,Std})/(0.95A_{NBS\,Std}) \times 1{,}000 \quad (19.2)$$

The principal modern radiocarbon standard ($A_{NBS\ Std}$) is NIST oxalic acid I ($C_2H_2O_4$), made from a crop of 1955 sugar beets. Ninety-five percent of the activity

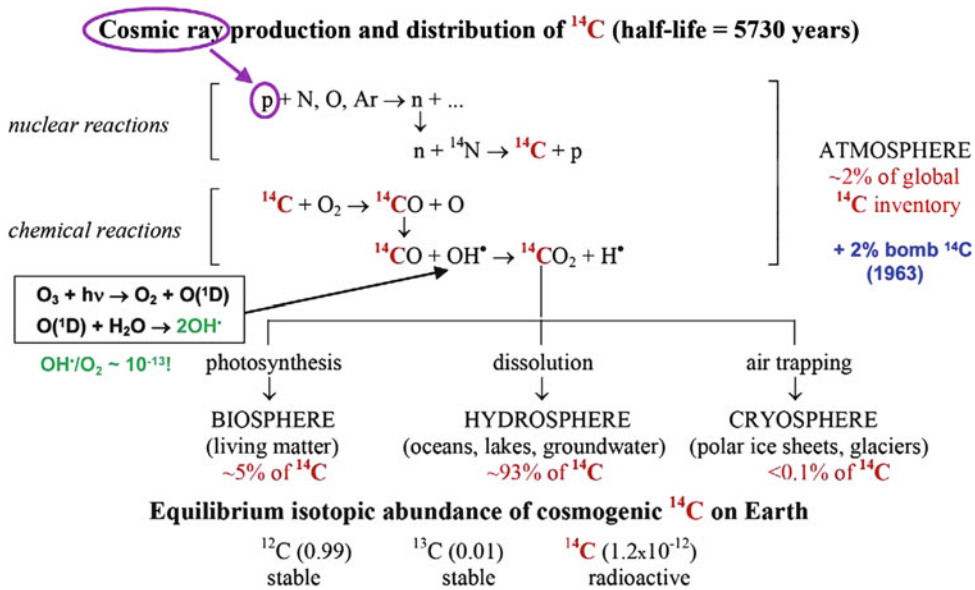

Fig. 19.2 Schematic presentation of the processes leading to the production and distribution of ^{14}C on earth. The sudden increase of ^{14}C in the atmosphere by nuclear weapons testing in the early 1960 is also indicated. (Kutschera 2010, used with permission)

of oxalic acid I from the year 1950 is equal to the measured activity of the absolute radiocarbon standard which is 1890 wood (chosen to represent the pre-industrial atmospheric $^{14}CO_2$), corrected for radioactive decay to 1950.

Furthermore, it is necessary to allow for ^{14}C differences produced by isotopic fractionation. This is achieved by use of the $^{13}C/^{12}C$ ratio, which is itself also expressed as enrichment:

$$\delta^{13}C(‰) = \left[\left(^{13}C/^{12}C\right)_{sample} - \left(^{13}C/^{12}C\right)_{standard}\right] / \left[\left(^{13}C/^{12}C\right)_{standard}\right] \times 1,000 \quad (19.3)$$

Normalized ^{14}C enrichments are then given by the formula:

$$\Delta^{14}C = \delta^{14}C - 2(\delta^{13}C + 25)(1 + \delta^{14}C/1{,}000)\ ‰ \quad (19.4)$$

19.3.2.1 Validating Global Ocean Carbon Model

The distribution of bomb-produced ^{14}C in the ocean has been summarized on the basis of radiocarbon measurements made during GEOSECS (Geochemical Ocean Sections Study), TTO (Transient Tracers in the Ocean), and SAVE (South Atlantic Ventilation Experiment) ocean survey programs. The inventory of bomb ^{14}C and the mean penetration depth of this tracer in the water column for the Atlantic (1972–1973), Pacific (1973–1974), and Indian (1977–1978) oceans have been published from the GEOSECS results. To eliminate the time difference, these bomb ^{14}C inventories are normalized to 1 January 1975. This represents the global spatial distribution of bomb ^{14}C tracer, which is required for calibration of ocean models, especially when these models are to be used for estimating the oceanic uptake of CO_2. In addition, results obtained from expeditions during later years from TTO in the northern and tropical Atlantic (1981–1982), and SAVE in the southern Atlantic (1987–1988) are also published by Broecker et al. (1995). This information depicts the temporal variations of the bomb ^{14}C distribution in the Atlantic Ocean. The evolution of bomb ^{14}C inventory in the ocean with time is another valuable piece of information for verifying the models of the global ocean carbon cycle (Peng et al. 1998).

19.3.2.2 Tracing Dissolved Organic Carbon Sinking in the Sea

According to Beaupre and Druffel (2009), dissolved organic carbon (DOC), is largely derived from the autochthonous production in the sun-lit surface ocean, and is the largest reservoir of reduced carbon in the ocean with its magnitude of about 685×10^{15} g C and is comparable to the carbon in the atmosphere in the form of CO_2. The 4,000–6,000 year ^{14}C ages of deep ocean DOC suggest that a significant portion cycles on longer time scales and ages during deep water transit. The processes that produce these old ages remain unknown. As a tracer of time and carbon sources, the ^{14}C content of marine DOC is a powerful tool for potentially constraining many of these uncertainties. They were able to infer the sinking of DOC from the surface ocean to depths of about 450 m on time scale of months based on the time series observations of $\Delta^{14}C$ of DOC between 1991 and 2004, and the magnitude and synchronicity of major $\Delta^{14}C$ anomalies (Beaupre and Druffel 2009).

19.3.2.3 Dating Marine Samples for the Recent Past ~60 Years with High Accuracy

Living organisms take up radiocarbon through the food chain and via metabolic processes. This provides a supply of ^{14}C that compensates for the decay of the existing ^{14}C in the organism, establishing equilibrium between the ^{14}C concentration in living organisms and that of the atmosphere. When an organism dies, this supply is cut off and the ^{14}C concentration of the organism starts to decrease by radioactive decay at a rate determined by the radiocarbon half-life. This rate is independent of other physical and environmental factors. The time t elapsed since the organism was originally formed can be determined from (19.5):

$$t = T_{1/2}/\ln 2 \times \ln(N_t/N_o) \quad (19.5)$$

where $T_{1/2}$ is the radiocarbon half-life, N_o is the original ^{14}C concentration in the organism and N_t is its residual ^{14}C concentration at time *t* (Hua 2009). This method has been utilized extensively for the climate proxies and dating older objects in archaeology. However, we would like to highlight the importance of bomb-derived ^{14}C as the anthropogenic ^{14}C

overwhelmed the naturally produced ^{14}C by masking its natural variability, and thus allowed dating objects of the recent past ~60 years with much greater accuracy than for ^{14}C age-dating conducted during the pre-bomb period, e.g., determination of age-depth model for a salt marsh (Marshall et al. 2007). As another example, accurate measurements of the age of fish provide valuable information for the sustainable management of fish stock in the sea (for dating of fish otoliths, see Chap. 37). Piner et al. (2006) collected otoliths from bocassio rockfish off the coast of Washington State of USA and determined their birth years and inferred that they can live at least 37 years. The age-structured stock assessment is helpful for the fish mangers to evaluate the sustainability of the fish populations in the region.

19.3.2.4 Tracing Source of Organic Matter in Estuary

Organic matter is one of the controlling factors determining the fertility and environmental quality of estuaries and coastal oceans. Organic matter may have its origin from in situ primary production, resuspension of the bottom sediment, and terrestrial detritus discharged from surface runoff through rivers and streams. The advantage of ^{14}C determinations over the use of ^{13}C as a marker for the source of organic material is the fact that ^{14}C age of biomass of short living organisms is, unlike-$\delta^{13}C$, the same for all organic constituents, because the effect of isotopic fractionation is removed by the normalization procedure used in ^{14}C age determination as described above. For example, Megens et al. (2001) were able to elucidate that particulate organic matter in the southern North Sea during winter is mainly derived from the resuspension from the bottom sediment by utilizing bomb-^{14}C signal.

19.3.3 Manganese (^{54}Mn)

^{54}Mn, ^{58}Co, ^{60}Co, ^{134}Cs and ^{137}Cs are among the common beta/gamma emitting radionuclides discharged under normal operating conditions by many nuclear facilities. For instance in 1995, these five isotopes accounted for about 68% of the non-tritium low-level radioactive liquid wastes from French 1,300 MW pressurized reactors. In addition to this radioecological aspect, the three elements selected present a special interest from a biological standpoint. Cs is biochemically analogous to K while Mn and Co are classified among the ten vital elements for life. Co is vital to many enzymatic systems and to the formation of noble molecules, such as vitamin B-12. Mn is a coactivator of such enzymes as transferases and decarboxylases, and is a constituent of several metalloenzymes, including pyruvate carboxylase and superoxide dismutase. Therefore, these radionuclides could be used to study metal physiology, e.g., trophic transfer factors, in biological organisms in the marine areas adjacent to the nuclear waste discharge facilities (Baudin et al. 2000).

19.3.4 Iron (^{55}Fe)

Introduction, formation, decomposition, dissolution, and sinking of particulate matter is largely responsible for the vertical segregation of biophilic chemical elements in the sea. The main aspects of particulate matter have been the size, settling rate, and physical, chemical and biological compositions. During the 1960, ^{55}Fe constituted one of the major radioactive isotopes present in atmospheric fallout. Although ^{55}Fe, which has a 2.4 year half-life, decays exclusively through electron capture and emits a very weak 5.9 keV X-ray, this isotope is of biological interest because Fe is an essential element for plant growth and is absorbed by red blood cells of animals. ^{55}Fe fallout from atmospheric weapons detonations was largely associated with aerosols as an amorphous oxide or as extremely small particulate species attached to the surfaces of large aerosol particles. The ^{55}Fe contained in these aerosols was more readily solubilized and became available to marine organisms than the stable iron in geological matrix of soil (Weimer and Langford 1978). Massic ^{55}Fe activity was utilized to obtain Fe-laden particle dynamics in the Pacific Ocean. Lal and Somayajulu (1977) found that ^{14}C-laden biogenic calcareous particles (~ 6 μm diameter) sank faster than ^{55}Fe-labeled small particles (~ 1 μm diameter) sinking to the depths of 2,500 m in the Pacific Ocean. And ^{55}Fe-labled particles sank faster than Pu isotope-labeled particles in the North Pacific Ocean (Livingston et al. 1987). These studies indicated that particulate carrier phase may be specific to each metallic element. Recently the role of iron in the photosynthesis of marine plant,

hence, its influence on the climate change has drawn considerable attention. Its role on the sequestration of atmospheric CO_2 received extensive interests from both scientific and commercial community (e.g., Betram 2010). In this context, biogeochemistry of iron in the sea could be elucidated using ^{55}Fe as a tracer at sites where it is released.

19.3.5 Cobalt (^{58}Co and ^{60}Co)

Controlled low level radioactive waste release from routine operation of nuclear power plants could be monitored using ^{60}Co and other radionuclides (^{137}Cs, ^{134}Cs) and their spatial gradients could be used for estimating the extent of discharge plume in the receiving water body and sediment budget (Olsen et al 1981). Cutshall et al. (1986) used ^{60}Co and ^{152}Eu to trace the Columbia River derived sediment in Quinault Canyon, Washington, USA by utilizing unusual, once-through, open-loop cooling system at the Hanford nuclear facility. Donoghue et al. (1989) have used ^{134}Cs to estimate sediment trapping behind the river dams located below the nuclear reactors as the affinity of cesium for sediment particles, illite mineral in particular, in the freshwater are very high and desorption does not occur. The presence of ^{60}Co in the bottom sediment was used to confirm a nuclear submarine reactor accident occurred in 1985 in Sterlok bay, Peter the Great Bay off Vladivostok (Tkalin and Chaykovskaya 2000).

19.3.6 Krypton (^{85}Kr)

^{85}Kr concentrations in the atmosphere and ocean have been increasing steadily since 1945 as a result of atmospheric release from nuclear power plants, plutonium production and nuclear waste processing facilities, and in atmospheric nuclear weapons tests. ^{85}Kr has a great potential as a tracer for ocean ventilation and water mass formation. There are two basic reasons for this: (1) ^{85}Kr enters the ocean by gas exchange with an equilibration time of 1 month or less. Hence nearly the entire ocean surface will be in equilibrium with the atmosphere, and the surface water concentration as a function of time at any location in the ocean can be accurately calculated from the documented atmospheric history (Winger et al. 2005; Kemp 2008) and krypton solubility data; and (2) Krypton is an inert gas and ^{85}Kr is absolutely conservative in seawater except for its radioactive decay. Smethie et al. (1986) were able to show that Norwegian Sea Deep Water forms from a mixture of Greenland Sea Deep Water and Eurasian Basin Deep Water. They estimated the volume transports for exchange between the surface and deep Greenland Sea and for exchange between the deep Greenland and deep Norwegian seas. They also estimated the residence time of water in the deep Greenland Sea with respect to exchange with surface water. As ^{85}Kr is introduced from the air, deep water sample for the gas analysis may be checked with its presence as an indicator of air contamination during sampling (Schlosser et al. 1995).

19.3.7 Strontium (^{89}Sr and ^{90}Sr)

Most of the ^{90}Sr fallout in surface waters is derived from global fallout. The interest in ^{90}Sr stems from the following: (1) ^{90}Sr is a high-yield product of U and Pu fission; (2) ^{90}Sr is a tracer for stable Sr, and Sr has similar properties as Ca; (3) ^{90}Sr is the most widely and carefully monitored fallout radionuclide in precipitation, aerosols, and soils. Indeed, the bomb test fallout of ^{137}Cs is calculated based on the monitored ^{90}Sr fallout, assuming constancy of the ^{90}Sr/^{137}Cs ratio, and (4) its moderate half-life of 28.9 years (Baskaran et al. 2009). In the year of 2000, total oceanic inventory of ^{90}Sr was estimated to be 189 PBq (37 kg) (Hamilton 2004) and it constitutes ca. 0.3×10^{-9} g ^{90}Sr/g Sr in the world ocean based on the average Sr concentration (8.7×10^{-5} mole/kg) and world ocean volume (1.37×10^{21} L) (Broecker and Peng 1982). ^{90}Sr largely resides in the water column with subsurface peak at ca. 300 m (Fig. 19.6) and very small fractions (0.02–0.04%) are buried in the sediment in the deep Pacific Ocean Basin (Lee et al. 2005). ^{90}Sr concentration in the surface 1 km depth decreased approximately 30% over the past 24 years (Fig. 19.3). As the environmental half-life of ^{90}Sr in the central NW Pacific Ocean is ca. 15 years (Povinec et al. 2005), ^{90}Sr would decrease to 0.1 Bq m^{-3} by 2060 (if there is no additional sources in the future), which would be difficult to measure with 50 L of seawater sample using oxalate precipitation method (Baskaran et al. 2009).

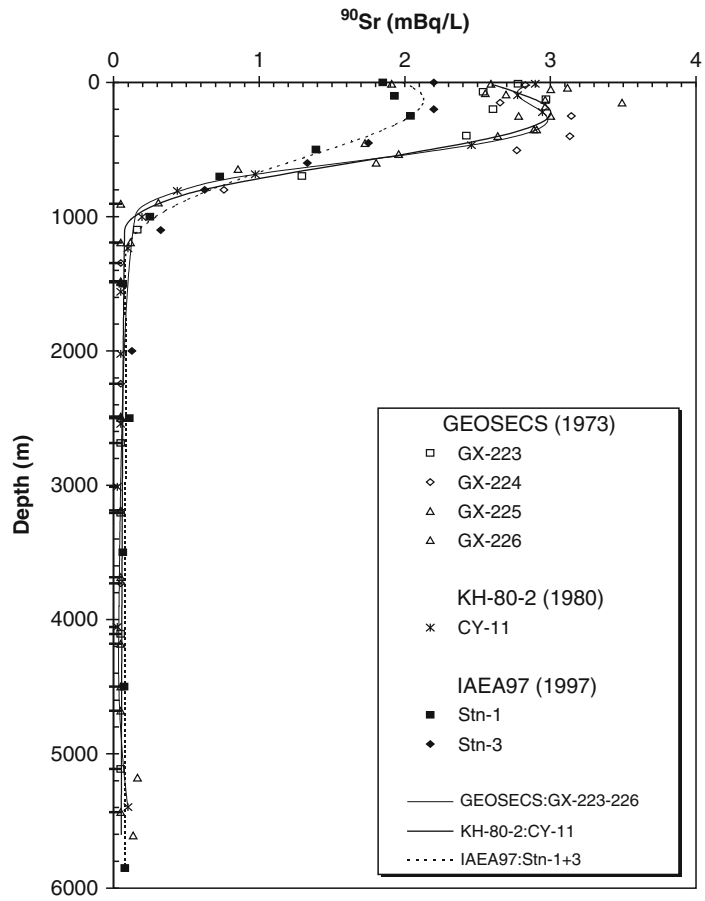

Fig. 19.3 ^{90}Sr concentration profiles in the central NW Pacific Ocean in 1997 (IAEA 1997) along with earlier GEOSECS (1973), KNORR (1978), Hakuho Maru (1980) measurements (Povinec et al. 2003, used with permission)

The residence time of stable Sr is ~ 5 × 10^6 year in the ocean, and several orders of magnitude longer than the global ocean turnover time (~ 1,500 years). The removal from the sea can be made through the formation of $SrCO_3$ (strontianite), $SrSO_4$ (celestite), and incorporated into Barite ($BaSO_4$) as impurities. $SrCO_3$ is formed when Sr is incorporated into coralline skeletons at sea. The sodium carbonate fortified seawater from which coral skeleton precipitates has a Sr/Ca ratio close to that of seawater (~0.8 × 10^{-2}), but it is depleted in Mg and Ba (Gaetani and Cohen 2006). Recently, it was shown that $SrCO_3$ mol percentage in coralline algae (rhodoliths) in coastal waters off Scotland closely followed the in situ temperature (Kamenos et al. 2008). Therefore, ^{90}Sr might be utilized as a paleothermometer for corals and other biogenic carbonates proxies.

Celestite is formed as major skeletons and cysts of acantharians, abundant planktonic protists. Settling skeletons of dead acantharians and acantharian cysts are readily dissolved because the ocean is undersaturated with respect to $SrSO_4$. Most oceanic water is undersaturated with respect to barite ($BaSO_4$), yet barite particles are ubiquitous throughout the water column in the ocean. Barite formation in the water column and its accumulation in sediments are closely related to export production of carbon. Sr is incorporated into barite precipitation (average 36.6 mmol Sr/mol Ba) (Paytan et al. 2007). However, the mechanism of barite formation has not been clearly understood yet. Three main hypotheses that have been proposed for barite formation in the oceanic water column include: (1) Barite is formed in microenvironments in which sulfate is enriched due to organic matter oxidation;

(2) A thermodynamically driven barite formation process in which the dissolution of acantharian celestite ($SrSO_4$), which is enriched in Ba ($BaSO_4/SrSO_4$), creates barium rich microenvironments conducive to barite precipitation; and (3) Barite is formed by Ba enrichment rather than SO_4^{2-} enrichments. It is reported that these proposed mechanisms for barite formation are not mutually exclusive. Acantharian dissolution within microenvironments appears to lead to $BaSO_4$ supersaturation and subsequent barite formation (Bernstein and Byrne 2004).

In case of a relatively fresh fission product mixture, another radiostrontium, ^{89}Sr with a half-life of 50.5 days, can also be present. As the fission yields of both ^{89}Sr and ^{90}Sr are known, their activity ratio can be applied in the dating of the fission product formation. According to UNSCEAR (2000), the $^{89}Sr/^{90}Sr$ activity ratio should be 188 just after a nuclear explosion (Paatero et al. 2010)

19.3.7.1 Quantifying Particle Removal

The disequilibrium between the soluble parent isotope ^{90}Sr ($t_{1/2}$ = 29.1 years) and its particle-reactive daughter ^{90}Y ($t_{1/2}$ = 64 h) has been used to estimate particle settling rates in freshwater systems (Orlandini et al. 2003) and in estuaries and the coastal ocean. Because of the short half-life (64 h) of ^{90}Y, this method could-be used to trace faster processes than what is possible using ^{238}U ($t_{1/2}$ = 4.468×10^9 years)^{-234}Th ($t_{1/2}$ = 24.1 days) disequilibria. However, in order to utilize ^{90}Y–^{90}Sr pair as a particle-cycling tracer, the particulate ^{90}Y (^{90}Sr likely negligible) and dissolved ^{90}Y needs to be separated immediately after sample collection and hence immediate filtration is required. The mathematical expressions to relate the measurements of ^{90}Sr–^{90}Y disequilibrium to the physical dynamics of particles and particle-reactive species are similar to expressions developed and applied to uranium– thorium disequilibria in the sea (19.6).

$$\lambda_p N_p = \lambda_d N_d + kN_d \tag{19.6}$$

Here λ_p and λ_d are the decay constants of the parent (here ^{90}Sr) and the daughter nuclide (^{90}Y), respectively. The N terms are the atom concentrations of the parent and daughter nuclides in the water column. The k term is the first-order net removal rate coefficient (nonradioactive) for the particle-active daughter nuclide. In (19.6), the advection (horizontal and vertical) and diffusion are neglected. Solving for the removal coefficient (residence time = 1/k) and converting to activities (A, expressed in Bq m^{-3}) by using the appropriate decay constants gives the following:

$$k = \lambda_d (A_p - A_d)/A_d \tag{19.7}$$

19.3.7.2 Tracing Water Mass Movement

Water column distribution of ^{90}Sr, ^{99}Tc, ^{129}I, ^{137}Cs, ^{238}Pu, ^{239}Pu, and ^{241}Am over time was used to estimate horizontal advection rates of various water masses in various parts of the ocean, for example, in the Arctic Ocean (Livingston et al. 1984), Adriatic Sea (Franić 2005), Norwegian Sea (Yiou et al. 2002), and Sulu Sea (Yamada et al. 2006).

Also, ^{90}Sr activity in the river varies depending upon the watershed soil and denudation characteristics in its watershed, and could serve as a source indicator in the estuary. For example, ^{90}Sr activity in the Danube River was 15–30 times lower than that of Dneiper River in the north-west Black Sea. Based on this information, Stokozov and Buesseler (1999) constructed a water mixing model using ^{90}Sr and salinity as water mass tracers for the northwest Black Sea. Present distribution of ^{90}Sr also serves as the benchmark to assess future spreading of radionuclides for specific release scenarios. Gao et al. (2009) modeled the difference between the present-day and the 2 × atmospheric CO_2-warming scenario runs for the accidental releases of ^{90}Sr in the Ob and Yenisey rivers and indicated that more of the released ^{90}Sr would be confined to the Arctic Ocean in the global warming run, particularly in the coastal, non-European part of the Arctic Ocean.

19.3.8 Ruthenium (^{103}Ru and ^{106}Ru)

^{103}Ru and ^{106}Ru fallout radionuclides released from the Chernobyl accident along with other gamma-emitting fallout radionuclides, ^{134}Cs, ^{137}Cs, ^{110m}Ag, were used to quantify water mass movement in the seas. Carlson and Holm (1992) measured the concentrations of these nuclides in marine plant, *Fucus vesiculosus* L. in the

Baltic Sea area following the Chernobyl accident. The activity ratios of $^{106}Ru/^{137}Cs$ and $^{144}Ce/^{137}Cs$ in sediment trap and suspended particles were utilized to distinguish the particles laden with Chernobyl Cs ($^{134}Cs/^{137}Cs = 0.5$) and earlier global fallout ($^{134}Cs/^{137}Cs = 0.0$) in the Black Sea (Buesseler et al. 1990).

19.3.9 Antimony (^{125}Sb)

Antimony-125 is a conservative tracer. A large set of ^{125}Sb data collected from the English Channel and southern North Sea between 1987 and 1994 have been utilized to validate hydrodynamic model in this region (du Bois and Dumas 2005; du Bois et al. 1995). For the field validation with tracers, the coverage of the spatial and temporal tracer concentrations with high accuracy is required. The ideal water mass tracers should show conservative behavior in the water mass, i.e., neither fixed by environmental components (sediment, living species) nor modified during its stay in seawater, and when subsequently diluted, it must be measurable at several hundred or thousand kilometers from its point of discharge. Good tracers must have only one or a set of well-defined and characterized input functions and their flow must be well tracked. In this context, anthropogenic radionuclides released by nuclear fuel reprocessing plants fully meet these specifications if their half-life is long enough compared to the transit-times in the ocean basin. Since 1960, large-scale studies have been chiefly concerned with ^{137}Cs, a point source tracer due to the discharge from the nuclear fuel reprocessing plant at Sellafield on the Irish Sea. Other tracers, namely ^{134}Cs, ^{90}Sr and ^{99}Tc, ^{125}Sb and $^{239+240}Pu$ have also been used to monitor the transport of water masses. For example, dispersion of a water from the Rhone River into the coastal Mediterranean Sea was modeled using ^{125}Sb, ^{137}Cs and $^{239+240}Pu$ (Periáñez 2005).

19.3.10 Iodine (^{129}I)

In the terrestrial and marine environment, natural levels of ^{129}I (cosmogenic origin) have been overwhelmed by a build-up of ''new'' ^{129}I, a product of the nuclear age. Much of this new ^{129}I has entered the ocean and is now found in its upper layers. Using ^{129}I as a point source tracer due to the discharge from the nuclear fuel reprocessing plants, it has been employed as an oceanographic water mass tracer to determine transit time scale based on the horizontal concentration gradients from the point of discharge. ^{129}I has also been used as a tracer for monitoring nuclear activities, including nuclear safeguard investigations. Furthermore, the differences in the $^{129}I/^{137}Cs$ and $^{129}I/^{99}Tc$ activity ratios of reprocessed and unprocessed nuclear wastes are also utilized as markers to distinguish water masses because of their unique chemical properties (e.g., solubility, volatility) and high sensitivity of detection. The activity ratio $^{129}I/^{137}Cs$ was used to distinguish between accidental or deliberate discharges of these two types of radioactive wastes to the ocean (e.g., Raisbeck and Yiou 1999).

During primary production, iodine is incorporated in marine organic matter and migrates through the food chain. The $^{129}I/^{127}I$ atom ratio in marine organics therefore reflects the value found in the ocean's photic zone when the organic matter formed. Because the $^{129}I/^{127}I$ atom ratio in any well-mixed marine basin has increased rapidly since the advent of the nuclear age, establishing the buildup pattern of ^{129}I in that basin's surface waters would allow us to ''date'' the time of formation of any organic matter in the euphotic zone, provided we can obtain an adequate amount of iodine from samples (Schink et al. 1995). Measurement of this ratio currently requires the use of accelerator mass spectrometer (AMS).

19.3.11 Cesium (^{134}Cs and ^{137}Cs)

Cesium is an alkali metal existing as the Cs^+ ion in the oceans. Similar to other alkali metals (e.g., potassium), cesium is conservative in seawater (Brewer et al. 1972). In terrestrial environment, Cs is strongly associated with soil and sediment particles. K_d values for Cs in freshwater environments are large and on the order of $1–5 \times 10^5$. This value decreases substantially as particulate matter is delivered to the oceans via rivers and estuaries. As salinity increases, so too does competition for sediment sorption sites from other cationic species such as K^+, resulting in desorption of cesium. In pelagic environments, K_d is observed to be significantly lower and has been reported to vary

between 4×10^2 and 2×10^4 L kg^{-1} (IAEA 2004), with lower end in the Black Sea (Topcuoğlu et al. 2002).

In the year of 2000, total oceanic inventory of ^{137}Cs was estimated to be 300 PBq (93 kg) (Hamilton 2004) and it constitutes ca. 0.2×10^{-12} g ^{137}Cs/g Cs in the world ocean based on the average Cs concentration of 2.3×10^{-9} mole/kg and world ocean volume of 1.37×10^{21} L (Broecker and Peng 1982). ^{137}Cs largely resides in the water column with subsurface peak at ca. 200 m and very small fractions (0.01–0.12%) are buried in the sediment in the deep Pacific Ocean Basin (Lee et al. 2005). ^{137}Cs concentration in the surface 1 km depth decreased approximately 40% over the past 24 years (Fig. 19.4). As the environmental half-life of ^{137}Cs in the central NW Pacific Ocean is ca. 24 years (Povinec et al. 2005), ^{137}Cs would decrease to ca. 0.1 Bq m^{-3} by 2108, which would be difficult to measure with current AMP precipitation method (Baskaran et al. 2009).

19.3.11.1 Utilizing $^{134}Cs/^{137}Cs$ Activity Ratios for Estimating Water Transit Time in the Arctic

One of the most significant point source discharges of anthropogenic radionuclides in the ocean is the Sellafield reprocessing plant (formerly Windscale) UK into the Irish Sea since 1952 in the North Atlantic. The reprocessing waste from La Hague, north-west France discharging into the English Channel since 1966 is relatively small compared to Sellafield (Kershaw and Baxter 1995). The contribution of La Hague to the marine inventory of ^{137}Cs, ^{90}Sr, ^{99}Tc and Pu was estimated to be 2.3, 12.2, 12.6 and 0.4%, respectively, of the Sellafield releases (Kershaw and Baxter 1995). The discharge of anthropogenic radionucldies resulted in substantial increase in their inventories in the North Atlantic and its marginal seas. The soluble radionuclides (^{90}Sr, ^{99}Tc, ^{129}I, ^{134}Cs, ^{137}Cs) released from Sellafield are carried northwards out of the Irish Sea

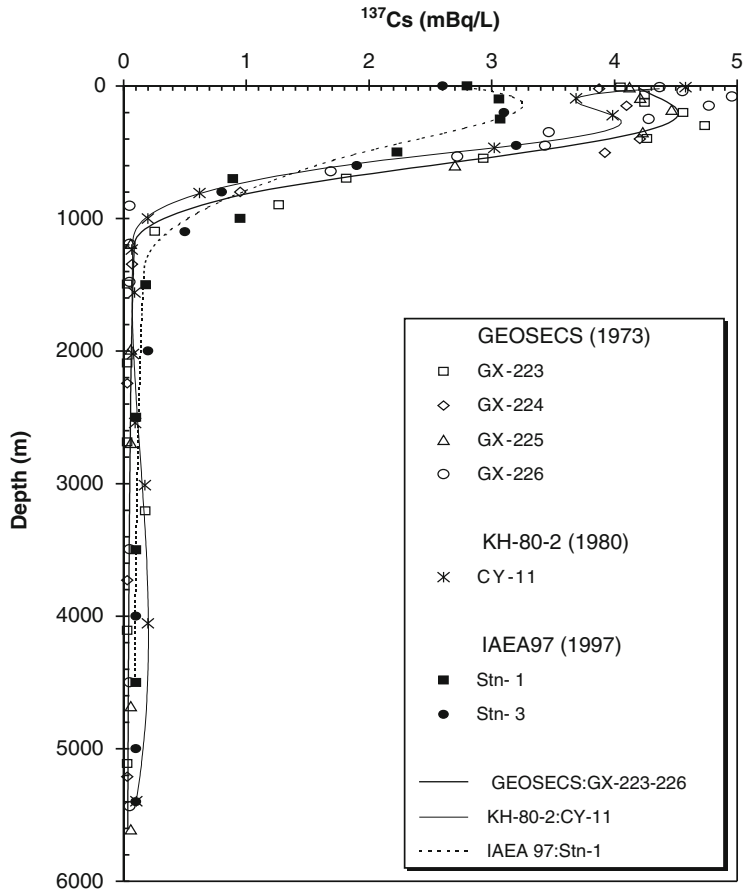

Fig. 19.4 ^{137}Cs profiles in the central NW Pacific Ocean in 1997 (IAEA 1997) along with earlier GEOSECS (1973), KNORR (1978), Hakuho Maru (1980) measurements (Povinec et al. 2003, used with permission)

via the North Channel, and flow around the coast of Scotland into the North Sea and then in the Norwegian Coastal Current (NCC). This NCC branches off northern Norway with one branch passing through eastwards into the Barents Sea (Vakulovsky 1987) and other current becomes the West Spitzbergen Current, passing through the Fram Strait into the Nansen Basin (Holm et al. 1983; Kautsky 1988; Smith et al. 1990); Kershaw and Baxter 1995). Using $^{134}Cs/^{137}Cs$ ratios at the source, one can determine the transit time of water masses from the discharge point to the Arctic Ocean. If R_0 and R_t are the $^{134}Cs/^{137}Cs$ activity ratios at the discharge point in Sellafield and at a point in the middle of Nansen Basin, then,

$$R_t = R_0 \exp(\lambda_{137} - \lambda_{134})t \qquad (19.8)$$

From this, the transit time (t) can be calculated as follows:

$$\tau = 1/(\lambda_{134} - \lambda_{137}) \times \ln(R_0/R_t) \qquad (19.9)$$

λ_{134} and λ_{137} are the decay constants of ^{134}Cs and ^{137}Cs, respectively. There is no other background ^{134}Cs, but there are background ^{137}Cs derived from the global fallout. At the time of sampling (1970), the background ^{137}Cs due to global fallout was in the range of 3–5 Bq m^{-3} at the corresponding latitudes, whereas levels at >120 Bq m^{-3} occurred in the northern Scottish waters. Equation (19.9) assumes the following: (1) the decrease in $^{134}Cs/^{137}Cs$ is only due to radioactive decay as the water mass moves; (2) there is no preferential removal of ^{134}Cs or ^{137}Cs; and (3) the change in $^{134}Cs/^{137}Cs$ activity ratio due to mixing with ^{134}Cs depleted water is negligible and the ^{137}Cs contribution from the global fallout to the sample collected is negligible. Using the $^{134}Cs/^{137}Cs$ ratios, the transit times were calculated to be 5–6, 7, and 7–9 years in North Cape, Svalbard, East Greenland, respectively (Kautsky 1988). This range of transit time is comparable to the advective time for transport around the perimeter of the Arctic Ocean from the Santa Anna Trough to the southern Canada Basin (~6,000 km) of 7.5 years obtained using H-3-He-3 and chlorofluorocarbon data (Mauldin et al. 2010). These values agree well with the values reported based on ^{137}Cs and ^{99}Tc (summarized in Kershaw and Baxter 1995). The transit time from La Hague to the Arctic is expected to be 3–4 years, about 2 years shorter than that reported for Sellafield (Kershaw and Baxter 1995).

19.3.11.2 Tracing Deep Water Formation Originated from the Regional Climate Change

The understanding of the deep water formation or intermediate water formation in the ocean is very important to understand the oceanic response due to climate change and vice versa. Sinking of surface water (formation of intermediate and deep water) is largely induced by the intense evaporation and cooling forced by regional climate, and it was generally studied using hydrographic observation such as temperature, salinity and dissolved oxygen. However, these hydrographic variables provide no direct information on the timing and duration of the sinking events. A time series measurement of ^{90}Sr and ^{137}Cs in deep waters could give direct information on the deep water formation. In the Mediterranean Sea, deep water formation occurring in the eastern part of the sea shifted from the southern Adriatic Sea to the Aegean Sea largely during 1989–1995 with exceptional severe winter in 1991–1993, known as Eastern Mediterranean Transient (EMT). The deep water formation in the Aegean Sea was relaxed partially by 1995. The deep penetration of the Aegean surface water was confirmed using time series depth distributions of ^{137}Cs in the water column collected over the period of 1975–1999 by Delfanti et al. (2003). They also utilized the ^{90}Sr-poor water formed during Chernobyl accident in 1986. In the Eastern Mediterranean Sea, ^{137}Cs concentration at 2,000 m depth was found to be ca. 1 and 3 Bq m^{-3} in 1977 and 1995, respectively. The activity ratio of $^{137}Cs/^{90}Sr$ in the surface water of the Mediterranean was 1.54 and 12 (in 1986) for the previous global fallout contained water and Chernobyl fallout contained water, respectively. This difference in the $^{137}Cs/^{90}Sr$ activity ratio is used to distinguish the water mass laden with ^{90}Sr-poor Chernobyl originated ^{137}Cs (high $^{137}Cs/^{90}Sr$ ratio) in 1986 from ^{90}Sr rich previous global fallout ^{137}Cs (low $^{137}Cs/^{90}Sr$ ratio) in the early 1960.

Miayo et al. (2000) found the timing of the deep water formation in a large marginal sea in the Northwest Pacific Ocean, East Sea (Sea of Japan) using historical ^{137}Cs profiles collected over the period of

1976–1996. They found that ^{137}Cs concentrations in the upper 200 m layer decreased with time, while those in the deeper layers below 1,500 m depth sharply increased during the period of 1985–1995, accompanied with the increase of the ^{137}Cs inventory. They further identified the area of deep water formation in this period being in the deep Japan Basin off the Peter the Great Bay, Vladivostok, Russia.

19.3.11.3 Tracing Ice Rafted Sediment in the Polar Seas

Sea ice in the polar region is one of the most important transport vectors of terrestrial material to the interior of the ocean. Terrestrial material is incorporated into the sea ice in the coastal areas when it forms and released at farther distances in the Arctic when it melts. In some cases, sea ice melts and the ice-rafted sediments (IRS) are retained in the melt ponds and during early fall, it refreezes. About 15% of the IRS are released during one freeze-melt cycle (details given in Kaste and Baskaran, Chap. 5 in this volume). From the measurements of ^{137}Cs in sea ice sediments, it was found that there is no enrichment of ^{137}Cs or Pu while one to two orders of magnitude enrichment was found for other atmospherically-delivered radionuclides such as ^{7}Be and ^{210}Pb (Meese et al. 1997; Cooper et al. 1998; Landa et al. 1998; Baskaran 2005; Masque et al. 2007). The ^{239}Pu/^{240}Pu atom ratios in the IRS were found to be ~0.18, suggesting that most of the Pu were derived from the global fallout (Masque et al. 2007).

19.3.12 Neptunium (^{237}Np)

Np is also an actinide element, but it differs from plutonium in that it is most likely present as the highly soluble Np(V) as NpO_2^+ (Keeney-Kennicutt and Morse 1984). While it can be present as Np(IV), it is proposed that Np (IV) in this form is rapidly oxidized to Np(V) under normal seawater conditions (McCubbin and Leonard 1997; Pentreath et al. 1986). K_d value of 1×10^3 kg L^{-1} has been reported for Np in coastal sediments. In the open ocean, ^{237}Np is thought to behave conservatively. Livingston et al. (1988) used fallout and Sellafield derived ^{137}Cs and ^{90}Sr to study ventilation and circulation processes in the Mediterranean and the Arctic Seas and documented their input into the North Atlantic Deep Water. ^{237}Np may have similar applications, with added benefits of a significantly longer half-life (2.14×10^6 years) and measurement by ICP-MS which allows lower levels of detection as compared to traditional radio-counting methods for ^{137}Cs and ^{90}Sr (i.e., gamma and beta counting). Furthermore, with the isotopic composition of the main sources of contamination well characterized, water column ^{237}Np inventories and ^{237}Np/^{239}Pu and ^{237}Np/^{137}Cs inventory ratios may be useful for identifying non-fallout sources of contamination and providing additional insight into water column scavenging processes.

19.3.13 Plutonium (^{239}Pu and ^{240}Pu)

Plutonium is an actinide element. Although Pu can exist in four oxidation states in natural environment, it is thought to exist in the oceans predominantly in two oxidation states, the particle reactive Pu(IV) as Pu$(OH)_4$ and the relatively soluble Pu(V) as PuO_2^+ (Sholkovitz 1983; McMahon et al. 2000). In many publications, the Pu(III) and Pu(IV) are grouped together as the reduced forms having average K_d values of 2.5×10^6 kg L^{-1} and Pu(V) and Pu(VI) are grouped together as the oxidized forms having average K_d values of 1.5×10^4 kg L^{-1} (Nelson and Lovett 1978).

Much of the published plutonium data is based on alpha spectrometry, which cannot resolve ^{240}Pu (5.168 MeV (73.5%), 5.123 MeV (26.4%)) from ^{239}Pu (5.157 MeV (73.3%), 5.144 MeV (15.1%), 5.106 MeV (11.5%)) and is usually reported as the sum of the ^{239}Pu and ^{240}Pu activity (i.e., ^{239,240}Pu). The average ^{239,240}Pu/^{137}Cs activity ratio of the global fallout is well documented to be 0.026 ± 0.01 (decay corrected to 1 Jan 2010) (Koide et al. 1977; Koide et al. 1975; Krey et al. 1976). More sensitive mass spectrometric techniques (e.g., ICP-MS and TIMS) have the ability to resolve the different isotopes of plutonium (details given in Chap. 18). Kelley et al. (1999) have shown that the atom ratios ^{240}Pu/^{239}Pu, ^{237}Np/^{239}Pu, and ^{241}Pu/^{239}Pu in soils contaminated by global fallout exhibit relatively little variation globally. Their average ratios in global fallout for the Northern Hemisphere are 0.180 ± 0.014, 0.480 ± 0.070, and $(2.44 \pm 0.35) \times 10^{-3}$, respectively (Chap. 20). Several studies have documented

lower plutonium isotopic ratios in debris originating from low-yield nuclear tests conducted at the Nevada Test Site to have an average $^{240}Pu/^{239}Pu$ ratio of about 0.035 (Buesseler and Sholkovitz 1987; Krey et al. 1976; Perkins and Thomas 1980).

In the year of 2000, total oceanic inventory of ^{239}Pu and ^{240}Pu are estimated to be 6.5 PBq (2,820 kg) and 5.4 PBq (632 kg), respectively (Hamilton 2004). $^{239+240}Pu$ largely resides in the water column with subsurface peak at ca. 600 m depth (Fig. 19.5) and substantial fractions (30–112%) are buried in the sediment in the deep Pacific Ocean Basin (Lee et al. 2005). The $^{239+240}Pu$ profiles in the central NW Pacific Ocean indicate that the subsurface maximum of Pu concentration over the past 24 years decreased by a factor of ca. 4 and the subsurface peaks moved to deeper water from ca. 450 to ca. 800 m and they were getting less sharp and more wide (Fig. 19.6). However, the stations located in the west-ward flowing North Equatorial Current (NEC) with very low biological activity showed no temporal changes in the vertical profiles of $^{239+240}Pu$ over the last 24 years (Povinec et al. 2003). The persistence of subsurface Pu peak appears to be correlated with the water density gradient (Wong et al. 1992). As the environmental half–life of $^{239+240}Pu$ in the central NW Pacific Ocean is ca. 7 years (Povinec et al. 2005), $^{239+240}Pu$ would decrease to less than 1 mBq m^{-3} by 2035, which would be difficult to measure with a conventional 60 L water volume and alpha spectrometry (Baskaran et al. 2009). Similar observation was made for the Santa Monica and San Padro Basins off California by Wong et al. (1992).

19.3.13.1 Tracing Provenances and Fates of Nuclear Fallout in the Ocean

Buesseler and Sholkovitz (1987) used Pu to document the input of both global stratospheric fallout and tropospheric fallout (derived from tests conducted at the Nevada Test Site) to North Atlantic sediments. They found the $^{240}Pu/^{239}Pu$ atom ratios ranged from ~ 0.18 on the shelf to ~ 0.10 at 5,000 m in the solid phase and

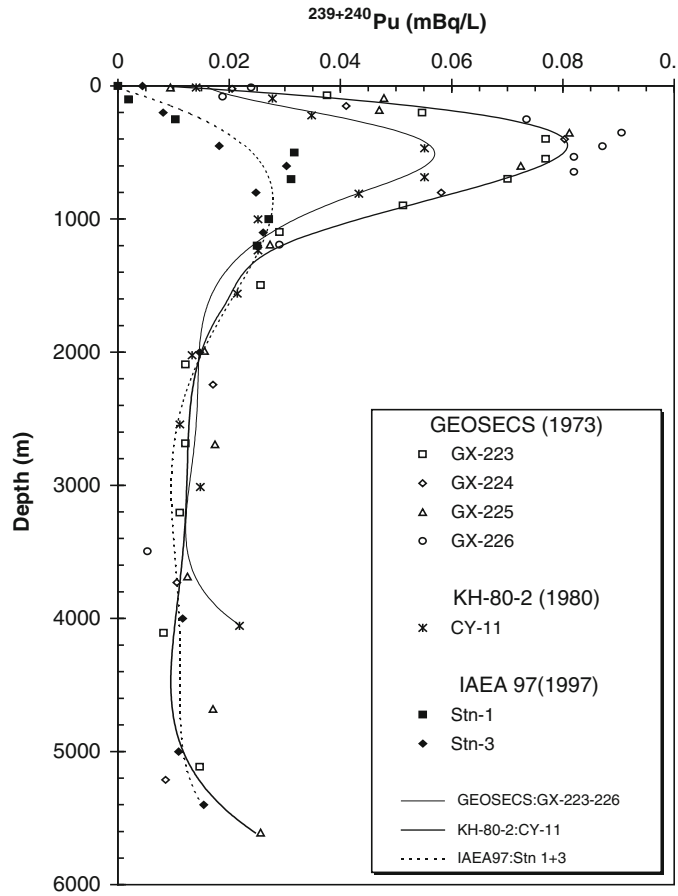

Fig. 19.5 $^{239,240}Pu$ profiles in the central NW Pacific Ocean in 1997 (IAEA 1997) along with earlier GEOSECS (1973), KNORR (1978), Hakuho Maru (1980) measurements (Povinec et al. 2003, used with permission)

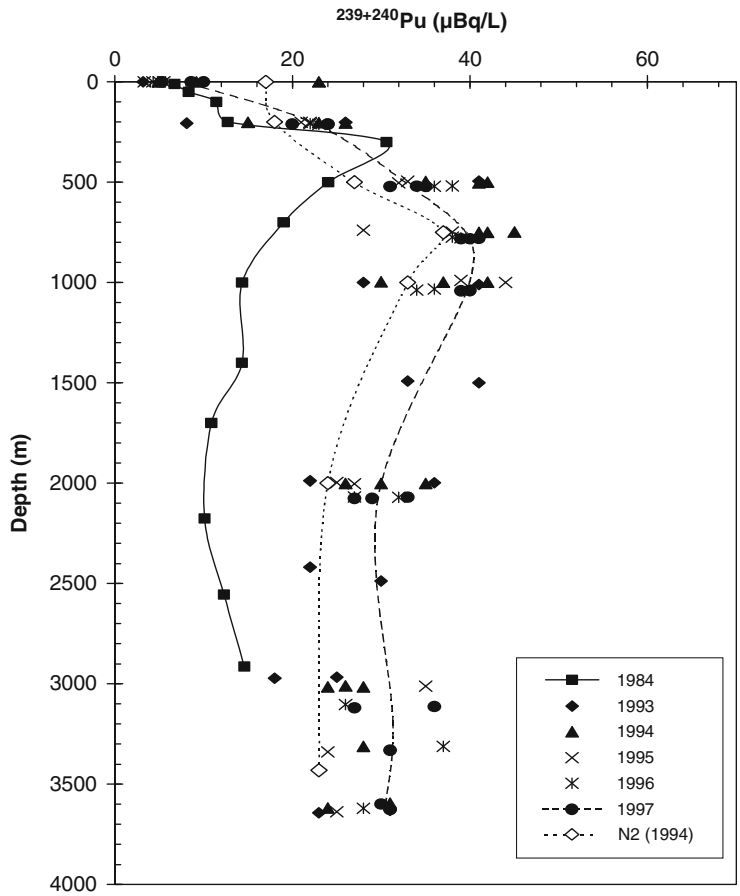

Fig. 19.6 Depth distribution of dissolved $^{239+240}$Pu concentrations over 1984–1997 in the Sea of Japan (East Sea) (from IAEA 2005). The time-series measurements were not done in a single fixed station

~ 0.18 in the pore water phases of bottom sediments collected from a transect between Woods Hole and Bermuda in the 1950 and early 1960. Based on the Pu isotopic composition, they were able to infer that there have been at least two distinct sources of fallout Pu in this region: one is global fallout (^{240}Pu/^{239}Pu ~ 0.18) and another tropospheric fallout from the Nevada Tests (^{240}Pu/^{239}Pu ~ 0.035), in which Pu derived from the Nevada Tests fallouts have been much more efficiently removed from the water column to deep-sea sediments and they were more refractory relative to Pu from global fallout.

19.3.13.2 Tracing Subtropical Water Movement in the Pacific Ocean

Although the entire surface of the Earth has been contaminated with radioactive fallout due to the atmospheric nuclear weapons tests conducted from 1945 to the early 1980, radioactive contamination in the Pacific Ocean is different from the rest of the world ocean. The earlier nuclear tests were dominated by the U.S. at the Pacific Proving Ground (close-in fallout, atom ratio of ^{240}Pu/^{239}Pu >0.3) in the 1950, whereas the later tests were largely by the former Soviet Union (stratospheric fallout, atom ratio of ^{240}Pu/^{239}Pu ~ 0.18) in 1961 and 1962. Stratospheric fallout from the atmospheric nuclear tests virtually ceased in the early 1980. Most of the terrestrial Pu contaminations in the world are largely originating from the former USSR nuclear tests. However, the Pu signal in seawater collected in early 2000 from the Pacific Ocean revealed that it was decoupled from that of the adjacent terrestrial environment and the data from the Pacific water has shown that US signal was found even off the Aleutian Chain, several thousand kilometers away from the Proving Ground.

The seawater in the Pacific Ocean had received close-in fallout in the 1950 and the stratospheric

fallout in the 1960. The earlier work (e.g., Noshkin et al. 1975; Buesseler 1997) showed that the $^{239}Pu/^{240}Pu$ atom ratios in the Pacific surface seawater had changed from the U.S. signal of >0.3 in the 1950 to a former Soviet signal in the 1960 and returned to the U.S. signal in the early 2000. No observations have been made between the late 1970 and the early 2000, which could be filled using samples from coral skeletons or archived seawater.

The Pu isotopic signature in the region is a potent and unique tracer to distinguish among the different sources of Pu, as well as to understand the variations of $^{239}Pu/^{240}Pu$ ratios through time (Ketterer et al., Chap. 20). The US Proving Grounds in the Pacific continue to export Pu with high $^{240}Pu/^{239}Pu$ ratio, mainly originated from the nuclear weapons tests in 1950, through the leaching of contaminated carbonate species deposited in the ocean. The massive (dome-shaped) coral *Porites* found throughout the northern tropical Pacific Ocean will allow us to reconstruct the Pu signal in surface waters spanning the last 50 years. By determining atom ratios of $^{240}Pu/^{239}Pu$ recorded in coral cores and dating the corals using the $^{210}Pb/^{226}Ra$ disequilibria (details on dating of corals is given in Chap. 37), we may be able to accomplish a better understanding of the mixing and circulation of waters between the Warm Pool and adjacent water masses in the Northwest Pacific Ocean. However, this application has not been fully realized yet (Hong et al. 2004).

19.3.13.3 Tracing Material Exchange Between Ocean and its Margins

The dissolved ^{230}Th activity concentration increases with depth in agreement with the balance between the in situ production from the dissolved ^{234}U and the scavenging of ^{230}Th on sinking particles generally in the ocean. However, a significant fraction of dissolved ^{231}Pa (daughter of ^{235}U) and some dissolved ^{230}Th were found to be exported from area of low particle flux to area of high particle flux where ^{230}Th and ^{231}Pa are efficiently scavenged by settling particulate matter to the sea floor. This process became widely known in the early 1980 as "boundary scavenging" because ocean boundaries/margins are generally areas with high biological productivity, high particle flux and high sediment accumulation. The concept of boundary scavenging was first applied to horizontal transport of ^{210}Pb (Spencer et al. 1981; Baskaran and Santchi 2002; Roy-Barman 2009). And enhanced deposition of fallout-derived Pu isotopes in ocean-margin sediments has also been reported (e.g. Koide et al. 1975).

In some ocean margins where large rivers are absent, e.g., East Sea (Sea of Japan), the oceanic $^{239+240}Pu$ is effectively scavenged through this boundary scavenging process and the deep waters become enriched with $^{239+240}Pu$ over time (Fig. 19.6) and the marginal sea is destined to continue to serve as a filter for all particle-reactive chemical materials introduced from incoming oceanic waters or atmosphere. This aspect should be investigated more fully in the future.

19.3.13.4 Identifying Subsurface Water Upwelling Areas in the Sea

Although both ^{137}Cs and $^{239+240}Pu$ radionuclides were injected into the ocean surface by similar processes, the oceanic behavior of plutonium and ^{137}Cs differ from each other. ^{137}Cs, most of which exists in a dissolved form, moves as water mass in the ocean, whereas oceanic behavior of $^{239+240}Pu$ is controlled both by water movement and adsorption onto the particles formed in situ or introduced and subsequently sinking to the deeper waters. Therefore, in the upper 1,000 m depths, ^{137}Cs concentration decreases exponentially with depth with surface maximum or subsurface maxima where surface water subducts. $^{239+240}Pu$ has increased with depth toward the subsurface maximum which lies about 500–800 m depth. Hirose et al. (2009) found that activity ratio of $^{239+240}Pu/^{137}Cs$ ($R_{Pu/Cs}$) increases with depth in the upper 100–1,000 m depth as follows:

$$R_{Pu/Cs} = R_{Pu/Cs,0}\exp(\lambda Z) \tag{19.10}$$

Where λ is the constant related to ocean biogeochemical process of water movement (downwelling and upwelling) and particle formation and destruction and Z is the water depth. They further noted that a half-generation depth of $^{239+240}Pu$, $Z_h = \ln 2/\lambda$, corresponds to the half-decrease depth of the particulate organic matter in the water column. As the ocean primary productivity depends on the upwelling

intensity of the nutrient-rich deep water, they found that Z_h is deep (~ 300 m) in the eutrophic subarctic Pacific and shallow (~ 100 m) in the subtropical North Pacific.

19.3.13.5 Constraining Sediment Accumulation and Mixing Rates

Particle reactive anthropogenic radionuclides (Table 19.1) has been utilized to determine sediment accumulation and mixing rates in the seafloor based on the input history and their half-lives as they often are adsorbed to the sediment irreversibly in the oceanic environment. Bomb-derived fallout radionuclide (^{137}Cs, $^{239+240}$Pu) peaks its concentration in 1963 in the Atlantic Ocean. However $^{239+240}$Pu peaked in 1954 in the Equatorial-North Pacific Ocean (Hamilton 2004) and the Antarctic Region (Koide et al. 1985) due to the close-in fallout in the Equatorial Pacific. Sediment accumulation rates may be calculated by assuming a fallout maximum in 1963 in the rapid sediment accumulating coastal ocean (e.g., Santschi et al. 2001) or sediment mixing rates may be calculated in the deep ocean basin where sediment accumulation rate is slower than mixing rate (e.g., Pacific Ocean, Cochran 1985).

19.3.14 Americium (^{241}Am)

Measurements of ^{241}Pu ($t_{1/2} = 14.3$ years) and its daughter product, ^{241}Am ($t_{1/2} = 433$ years) in the sediment sample can be used to establish the timing of the source term. Assuming that an initial activity of ^{241}Am in fallout debris is zero, the time elapsed since the Pu was placed, t, can be given by the radioactive decay equation governing the time-dependent activities $A_{Pu\text{-}241}$ and $A_{Am\text{-}241}$, respectively (19.11).

$$t = 1/(\lambda_{Pu-241} - \lambda_{Am-241}) \times \ln[1 + (\lambda_{Pu-241} - \lambda_{Am-241})A_{Am-241}/(\lambda_{Am241} - \lambda_{Pu-241})] \quad (19.11)$$

where λ is the radioactive decay constant ($0.693/t_{1/2}$) for a given isotope. In this way, Smith et al. (1995) reaffirmed that the underwater nuclear tests were conducted in Chernaya Bay to be in 1955 and 1957 (t obtained using (19.11) 36.6 ± 1.2 years can be compared to the time elapsed between 1955 and 1994 (or 1957 and 1994)).

19.4 Future Directions

A major portion of the remaining water soluble radionuclides (such as ^{90}Sr and ^{137}Cs) still exist in the water column with maximum in the surface or subsurface layer and hence these radionuclides can be utilized to study the geochemical pathways of their stable counterparts (e.g., pathways of Sr using ^{90}Sr as a tracer). About 60–70% of the total inventories of these nuclides derived from weapons testing have undergone radioactive decay, but the remaining portions continue to penetrate deeper water column in the ocean. Formation of barite minerals and the chemical reactions linked with such formation can be studied by using ^{90}Sr as a tracer.

Particle reactive anthropogenic radionuclides, e.g., Pu isotopes, continue to be transferred from the water column to the bottom sediments as enhanced in the ocean margins. Therefore, sediment inventories of these radionuclides would provide valuable temporal constraints on the boundary scavenging process occurring between ocean proper and its margins.

Slow movement of waters in the ocean, e.g., downwelling of surface water (deep water formation, drawdown of atmospheric CO_2), upwelling of subsurface water (supplying nutrient rich water to the surface, evasion of CO_2 to the atmosphere), spillover of deep water between basins are generally difficult to address using hydrographic variables such as temperature, salinity and stable isotopes of hydrogen and oxygen, where they have no time information. The current understanding of the spatial and temporal distribution in the sea and marine biogeochemistry of the well-studied anthropogenic radionuclides could serve to detect the slow movement of waters in the ocean. As the changes in slow movement of waters in the ocean are induced by the regional or global climate change, selected anthropogenic radionuclides, reviewed here, warrant a further investigation in a globally coordinated manner. The recently initiated GEOTRACES (an international study of the marine biogeochemical cycles of trace elements and their isotopes) could serve

a useful forum for this purpose (http://www.ldeo.columbia.edu/res/pi/geotraces/).

Acknowledgements The authors are grateful to Dr. Katusmi Hirose and an anonymous reviewer for providing valuable comments on the manuscript. This work was partially supported by Korea Ocean Research and Development PM55861 (GHH), was performed under the auspices of the U.S. Department of Energy by Lawrence Livermore National Laboratory in part under Contract W-7405-Eng-48 and in part under Contract DE-AC52-07NA27344 (TFH), Wayne State's Board of Governor's Distinguished Faculty Fellowship (MB). Copyright permission to reproduce here was generously granted for Table 19.2 and Figs. 19.1–19.5 from Elsevier Limited, UK and Table 19.3 from Terra Scientific Publishing Company, Japan.

References

Aarkrog A (1988) Worldwide data on fluxes of ^{239,240}Pu and ^{238}Pu to the ocean. In Inventories of selected radionuclides in the oceans. IAEA-TECDOC-481, 103–137

Aarkrog A (2003) Input of anthropogenic radionuclides into the world ocean. Deep-Sea Res II 50:2597–2602

Aoyama M, Hirose K, Sugimura Y (1991) The temporal variation of stratospheric fallout derived from the Chernobyl accident. J Environ Radioact 13:103–115

Assinder DJ (1999) A review of the occurrence and behavior of neptunium in the Irish Sea. J Environ Radioact 44:353–347

Baskaran M (2005) Interaction of sea ice sediment and surface sea water in the Arctic Ocean: evidence from excess ^{210}Pb. Geophys Res Lett: 32:L12601. doi:10.1029/2004GL022191

Baskaran M, Asbill S, Santschi PH, Davis T, Brooks JM, Champ MA, Makeyev V, Khlebovich V (1995) Distribution of ^{239,240}Pu and ^{238}Pu concentrations in sediments from the Ob and Yenisey rivers and the Kara Sea. Appl Radiat Isot 46:1109–1119

Baskaran M, Asbill S, Schwantes J, Santschi PH, Champ MA, Brooks JM, Adkins D, Makeyev V (2000) Concentrations of ^{137}Cs, ^{239,240}Pu, and ^{210}Pb in sediment samples from the Pechora Sea and biological samples from the Ob, Yenisey Rivers and Kara Sea. Mar Pollut Bull 40:830–838

Baskaran M, Hong GH, Santschi PH (2009) Radionuclide analyses in seawater. In: Wurl O (ed) Practical guidelines for the analysis of seawater. CRC, Boca Raton, pp 259–304

Baskaran M, Santschi PH (2002) Particulate and dissolved ^{210}Pb activities in the shelf and slope regions of the Gulf of Mexico waters. Cont Shelf Res 22:1493–1510

Baudin JP, Adam C, Garnier-Laplace J (2000) Dietary uptake, retention and tissue distribution of ^{54}Mn, ^{60}Co and ^{137}Cs in the rainbow trout (*Onchoryhynchus Mikiss* Walabaum). Water Resour 34:2869–2878

Beasley TM, Cooper LW, Grebmeier JM, Aagard K, Kelley JM, Kilius LR (1988) ^{237}Np/^{129}I atom ratios in the Arctic Ocean: has ^{237}Np from western European and Russian fuel reprocessing facilities entered the Arctic Ocean? J Environ Radioact 39:255–277

Beaupre SR, Druffel ERM (2009) Constraining the propagation of bomb-radiocarbon through the dissolved organic carbon (DOC) pool in the northeast Pacific Ocean. Deep-Sea Res I 56:1717–1726

Bernstein RE, Byrne RH (2004) Acantharians and marine barite. Mar Chem 86:45–50

Betram C (2010) Ocean iron fertilization in the context of the Kyoto protocol and the post-Kyoto process. Energy Policy 38:1130–1139

Bienvenu P, Cassette P, Andreoletti G, Be M-M, Comte J, Lepy M-C (2007) A new determination of ^{79}Se half-life. Appl Radiat Isot 65:355–364

Bowen VT, Noshkin VE, Livingston HD, Volchock HL (1980) Fallout radionuclides in the Pacific Ocean: vertical and horizontal distributions, largely from GEOSECS stations. Earth and Planet Sc Lett 49:411–434

Brewer PG, Spencer DW, Robertson DE (1972) Trace element profiles from the GEOSECS-II test station in the Sargasso Sea. Earth Planet Sci Lett 16:111–116

Broecker WS (1974) Chemical oceanography. Harcourt Brace Jovanovich, New York, 214p

Broecker WS (2003) Radiocarbon. In: Holland HD, Turekian KK (eds) Treatise in geochemistry, the atmosphere, vol. 4. Elsevier-Pergamon, Oxford, pp 245–260

Broecker WS, Peng TH (1982) Tracers in the sea. Eldigio, New York, p 690

Broecker WS, Southerland S, Smethie W, Peng TH, Ostlund G (1995) Oceanic radiocarbon: separation of the natural and bomb components. Global Biogeochem Cycles 9:263–288

Browne E, Firestone RB (1986) Table of radioactive isotopes. Wiley-Interscience, New York

Bruland KW (1983) Trace elements in seawater. In: Riley JP, Chester R (eds) Chemical oceanography, vol 8. Academic, London, pp 157–221

Buesseler KO (1997) The isotopic signature of allout plutonium in the North Pacific. J Environ Radioact 36:69–83

Buesseler KO, Livingston HD (1996) Natural and man-made radionuclides in the Black Sea. In: Guéguéniat P, Germain P, Métivier H (eds) Radionuclides in the oceans: Inputs and Inventories, Les Editions de physique, Europe Media Duplication S.A. Les Ulis, pp 199–217

Buesseler KO, Livingston HD, Honjo S, Hay BJ, Konuk T, Kempe S (1990) Scavenging and particle deposition in the southwestern Black Sea – evidence from Chernobyl radiotracers. Deep-Sea Res 37:413–430

Buesseler KO, Sholkovitz ER (1987) The geochemistry of fallout plutonium in the North Atlantic: II. ^{240}Pu/^{239}Pu ratios and their significance. Geochim Cosmochim Acta 51: 2623–2637

Byrne RH (2002) Inorganic speciation of dissolved elements in seawater: the influence of pH on concentration ratios. Geochem Trans 3:11–16

Carlson L, Holm E (1992) Radioactivity in *Fucus vesiculosus L.* from the Baltic Sea following the Chernobyl accident. J Environ Radioact 15:231–248

Chiappini R, Pointurier R, Milies-Lacroix JC, Lepetit G, Hemet P (1999) ^{240}Pu/^{239}Pu isotopic ratios and $^{239+240}$Pu total measurements in surface and deep waters around Muroroa and Fangataufa atolls compared with Rangiroa atoll (French Polynesia). Sci Total Environ 237(238):269–276

Cochran JK (1985) Particle mixing rates in sediments of the eastern equatorial Pacific: evidence from ^{210}Pb, ^{239,240}Pu and ^{137}Cs distributions at MANOP sites. Geochim Cosmochim Acta 49:1195–1210

Cooper LW, Larsen IL, Beasley TM, Dolvin SS, Grebmeier JM, Kelley JM, Scott M, Johnson-Pyrtle A (1998) The distribution of radiocesium and plutonium in sea ice-entrained Arctic sediments in relation to potential sources and sinks. J Environ Radioact 39:279–303

Cooper LW, Beasley T, Aagaard K, Kelley JM, Larsen IL, Grebmeier JM (1999) Distributions of nuclear fuel-reprocessing tracers in the Arctic Ocean: indications of Russian river influence. J Mar Res 57:715–738

Cundy AB, Croudace IW, Warwick PE, Oh JS, Haslett SK (2002) Accumulation of COGEMA-La Hague-derived reprocessing wastes in French salt marsh sediments. Environ Sci Technol 36:4990–4997

Cutshall NH, Larsen IL, Olsen CR, Nittrouer CA, DeMaster DJ (1986) Columbia River sediment in Quinault Canyon, Washington – Evidence from artificial radionuclides. Mar Geol 71:125–136

Delfanti R, Klein B, Papucci C (2003) Distribution of ^{137}Cs and other radioactive tracers in the eastern Mediterranean: relationship to the deepwater transient. J Geophys Res 108 (C9):8108. doi:10.1029/2002JC001371

Donoghue JF, Bricker OP, Oslen CR (1989) Particle-borne radionuclides as tracers for sediment in the Susquehanna River and Chesapeake Bay. Estuarine Coastal Shelf Sci 29:341–360

du Bois PB, Dumas F (2005) Fast hydrodynamic model for medium-and long-term dispersion in seawater in the English Channel and southern North Sea, qualitative and quantitative validation by radionuclide tracers. Ocean Modell 9:169–210

du Bois PB, Salomon JC, Gandon R, Guegueniat P (1995) A quantitative estimate of English Channel water fluxes into the North Sea from 1987 to 1992 based on radiotracer distribution. J Mar Syst 6:457–481

Emsley J (1989) The elements. Clarendon, Oxford, p 256

Franić Z (2005) Estimation of the Adriatic Sea water turnover time using fallout ^{90}Sr as a radioactive tracer. J Mar Syst 57:1–12

Gaetani GA, Cohen AL (2006) Element partitioning during precipitation of aragonite from seawater: a framework for understanding paleoproxies. Geochim Cosmochim Acta 70:4617–4634

Gao Y, Drange H, Johannessen OM, Pettersson LH (2009) Sources and pathways of ^{90}Sr in the North-Arctic region: present day and global warming. J Environ Radioact 100:375–395

Gray J, Jones SR, Smith AD (1995) Discharges to the environment from the Sellafield site, 1951–1992. J Radiol Prot 15:99–131

Hamilton TF, Milliès-Lacroix J-C, Hong GH (1996) ^{137}Cs(^{90}Sr) and Pu isotopes in the Pacific Ocean: sources and trends. In: Guéguéniat P, Germain P, Métivier H (eds) Radionuclides in the oceans. Inputs and Inventories. Les Editions de Physique, Les Ulis, pp 29–58

Hamilton TF (2004) Linking legacies of the cold war to arrival of anthropogenic radionuclides in the oceans through the 20th century. In: Livingston HD (ed) Marine radioactivity. Elsevier, Amsterdam, pp 23–78

Hirose K, Aoyama M, Povinec PP (2009) ^{239,240}Pu/^{137}Cs ratios in the water column of the North Pacific: a proxy of biogeochemical process. J Environ Radioact 100:258–262

Hirose K, Igarashi Y, Aoyama M, Miyao T (2001) Long-term trends of plutonium fallout observed in Japan. In: Kudo A (ed) Plutonium in the environment. Elsevier Science, Amsterdam, pp 251–266

Holm E, Persson BRR, Hallstadius L, Aarkrog A, Dahlgaard H (1983) Radiocesium and transuranium elements in the Greenland and Barents Seas. Oceanolog Acta 6:457–462

Hong GH, Baskaran M, Povinec PP (2004) Artificial radionuclides in the western North Pacific: a review. In: Shiyomi M, Kawahata H, Koizumi H, Tsuda A, Awaya Y (eds) Global environmental change in the ocean and on land. Terrapub, Tokyo, pp 147–172

Hou X, Roos P (2008) Critical comparison of radiometric and mass spectrometric methods for the determination of radionuclides in environmental, biological and nuclear waste samples. Anal Chim Acta 608:105–139

Hua Q (2009) Radiocarbon: a chronological tool for the recent past. Quat Geochronol 4:378–390

Hu QH, Weng JQ, Wang JS (2010) Sources of anthropogenic radionuclides in the environment: a review. J Environ Radioact 101:426–437

IAEA (2004) Sediment distribution coefficients and concentration factors for biota in the marine environment. Technical reports series No. 422, International Atomic Energy Agency, Vienna, p 93

IAEA (2005) Worldwide marine radioactivity studies (WOMARS). Radionuclide levels in oceans and seas. IAEA-TECDOC-1429. International Atomic Energy Agency, Vienna, p 187

Irlweck K, Hrnecek E (1999) ^{241}Am concentration and ^{241}Pu/$^{239(240)}$Pu ratios in soils contaminated by weapons-grade plutonium. Akamemiai Kiado, Budapest, pp 595–599

Jenkins WJ (2001) Tritium-helium dating. Encyclopedia of Ocean Sciences 6:3048–3056

Kamenos NA, Cusack M, Moore PG (2008) Coralline algae are global paleothermometers with bi-weekly resolution. Geochim Cosmochim Acta 72:771–779

Kafalas P, Irvine J Jr (1956) Nuclear excitation functions and thick target yields: (Cr^{+d}). Phys Rev 104:703–705

Kautsky H (1988) Determination of distribution processes, transport routes and transport times in the North Sea and the northern Atlantic using artificial radionuclides as tracers. In: Guary JC, Guegueniat P, Pentreath RJ (eds) Radionucludes: a tool for oceanography. Elsevier Applied Science, London, pp 271–280

Kelley JM, Bond LA, Beasley TM (1999) Global distribution of Pu isotopes and ^{237}Np. The Sci Total Environ 237(238):483–500

Keeney-Kennicutt WL, Morse JW (1984) The interaction of Np (V)O_2^+ with common mineral surfaces in dilute aqueous solutions and seawater. Mar Chem 15:133–150

Kemp RS (2008) A performance estimate for the detection of undeclared nuclear-fuel reprocessing by atmospheric ^{85}Kr. J Environ Radioact 99:1341–1348

Kenna TC, Sayles FL (2002) The distribution and history of nuclear weapons related contamination in sediments from the Ob River, Siberia as determined by isotopic ratios of plutonium and neptunium. J Environ Radioact 60:105–137

Kershaw P, Baxter A (1995) The transfer of reprocessing wastes from north-west Europe to the Arctic. Deep-Sea Res II 42:1413–1448

Ketterer ME, Szechenyi SC (2008) Determination of plutonium and other transuranic elements by inductively coupled plasma mass spectrometry: a historical perspective and new frontiers in the environmental sciences. Spectrochim Acta Part B 63:719–737

Kim CK, Kim CS, Chang BU, Choi SW, Chung CS, Hong GH, Hirose K, Igarashi Y (2004) Plutonium isotopes in seas around the Korean Peninsula. Sci Total Environ 318:197–209

Kirchner G, Noack CC (1988) Core history and nuclide inventory of the Chernobyl core at the time of accident. Nucl Saf 29:1–5

Koide M, Berine KK, Chow TJ, Goldberg ED (1985) The $^{240}Pu/^{239}Pu$ ratio, a potential geochronometer. Earth Planet Sci Lett 72:1–8

Koide M, Goldberg ED, Herron MM, Langway CC Jr (1977) Transuranic depositional history in South Greenland firn layers. Nat 269:137–139

Koide M, Griffin JJ, Goldberg ED (1975) Records of plutonium fallout in marine and terrestrial samples. J Geophys Res 80 (30):4153–4162

Krey PW, Hardy EP, Pachucki C, Rourke F, Coluzza J, Benson WK (1976) Mass isotopic composition of global fall-out plutonium in soil: Transuranium nuclides in the environment, San Francisco, CA, USA, pp. 671–678

Kutschera W (2010) AMS and climate change. Nucl Instrum Methods Phys Res B 268:693–700

Kuwabara J, Yamamoto M, Assinder DJ, Komura K, Ueno K (1996) Sediment profiles of ^{237}Np in the Irish Sea: estimation of the total amount of ^{237}Np from Sellafield. Radiochim Acta 73:73–81

Lal D, Somayajulu BLK (1977) Particulate transport of radionuclides ^{14}C and ^{55}Fe to deep waters in the Pacific Ocean. Limnol Oceanogr 22:55–59

Landa E, Reimnitz E, Beals D, Pockowski J, Rigor I (1998) Transport of ^{137}Cs and $^{239,240}Pu$ by ice rafted debris in the Arctic Ocean. Arct 51:27–39

Lee SH, Gastaud J, La Rosa JJ, Liong Wee Kwong L, Povinec PP, Wyse E, Fitfield LK, Hausladen PA, Di Tada LM, Santos GM (2001) Analysis of plutonium isotopes in marine samples by radiometric, ICP-MS and AMS techniques. J Radioanal Nucl Chem 248:757–764

Lee SH, Povinec PP, Wyse E, Pham MK, Hong GH, Chung CS, Kim SH, Lee HJ (2005) Distribution and inventories of ^{90}Sr, ^{137}Cs, ^{241}Am and Pu isotopes in sediments of the Northwest Pacific Ocean. Mar Geol 216:249–263

Lindahl P, Roos P, Holm E, Dahlgaard H (2005) Studies of Np and Pu in the marine environment of Swedish – Danish waters and the North Atlantic Ocean. J Environ Radioact 82:285–301

Linsalata P, Simpson HJ, Olsen CR, Cohen N, Trier RM (1985) Plutonium and radiocesium in the water column of the Hudson River estuary. Environ Geol Water Sci 7:193–204

Linsley G, Sjoblom K-L, Cabianca T (2004) Overview of point sources of anthropogenic radionuclides in the oceans. In: Livingston HD (ed) Marine radioactivity, vol 6, Radioactivity in the environment. Elsevier, Amsterdam, pp 109–138

Livingston HD, Buesseler KO, Izdar E, Konuk T (1988) Characteristics of Chernobyl fallout in the southern Black Sea. In: Guary J, Guegueniat P, Pentreath RJ (eds) Radionuclides: a tool for oceanography. Elsevier, Essex, UK, pp 204–216

Livingston H, Kupferman SL, Bowen VT, Moore RM (1984) Vertical profile of artificial radionuclide concentrations in the Central Arctic Ocean. Geochim Cosmochim Acta 48:2195–2203

Livingston HD, Mann DR, Casso SA, Schneider DL, Surprenant LD, Bowen VT (1987) Particle and solution phase depth distributions of transuranics and ^{55}Fe in the North Pacific. J Environ Radioact 5:1–24

Livingston HD, Povinec PP (2000) Anthropogenic marine radioactivity. Ocean Coastal Manage 43:689–712

Livingston HD, Povinec PP (2002) A millennium perspective on the contribution of global fallout radionuclides to the ocean science. Health Phys 82:656–668

Marshall WA, Gehrels WR, Garnett MH, Freeman SPHT, Maden C, Xu S (2007) The use of 'bomb spike' calibration and high-precision AMS ^{14}C analyses to date salt-marsh sediments deposited during the past three centuries. Quat Res 68:325–337

Masque P, Cochran JK, Hirschberg DJ, Dethleff D, Hebbeln D, Winkler A, Pfirman S (2007) Radionuclides in Arctic sea ice: tracers of sources, fates and ice transit time scales. Deep-Sea Res 154:1289–1310

Mauldin A, Schlosser P, Newton R, Smithie WM Jr, Bayer R, Rhein M, Peter JE (2010) The velociy and mixing time scale of the Arctic Ocean Boundary Current estimated with transient tracers. J Geophys Res 115:C08002. doi:10.1029/2009JC005965

McCubbin D, Leonard KS (1997) Laboratory studies to investigate short-term oxidation and sorption behabiour of neptunium in artificial and natural seawater solutions. Mar Chem 56:107–121

McMahon CA, Leon Vintro L, Mitchell PI, Dahlgaard H (2000) Oxidation-state distribution of plutonium in surface and subsurface waters at Thule, northwest Greenland. Appl Radiat Isot 52:697–703

Meese DA, Reimnitz E, Tucker WB III, Gow AJ, Bischoff J, Darby D (1997) Evidence for radionuclide transport by sea ice. Sci Total Environ 202:267–278

Megens L, van der Plight J, de Leeuw JW (2001) Temporal variations in ^{13}C and ^{14}C concentrations in particulate organic matter from the southern North Sea. Geochim Cosmochim Acta 65:2899–2911

Miayo T, Hirose K, Aoyama M, Igarashi Y (2000) Trace of the recent deep water formation in the Japan Sea deduced from historical ^{137}Cs data. Geophys Res Lett 27:3731–3734

Muramatsu Y, Rühm W, Yoshida S, Tagami K, Uchida S, Wirth E (2000) Concentrations of ^{239}Pu and ^{240}Pu and their isotopic ratios determined by ICP-MS in soils collected from the Chernobyl 30-km zone. Environ Sci Technol 34:2913–2917

Muramatsu Y, Hamilton T, Uchida S, Tagami K, Yoshida S, Rosbinson W (2001) Measurement of $^{240}Pu/^{239}Pu$ isotopic ratios in soils from the Marshall Islands using ICP-MS. Sci Total Environ 278:151–159

Nelson DM, Lovett MB (1978) Oxidation state of plutonium in the Irish Sea. Nat 276:599–601

Noshkin VE, Wong KM, Eagle RJ, Gatrousis C (1975) Transuranics and other radionuclides in Bikini lagoon. Concentration data retrieved from aged coral sections. Limnol Oceanogr 20:729–742

Noureddine A, Benkrid M, Maoui R, Menacer M, Boudjenoun R, Kadi-Hanifi M, Lee SH, Povinec PP (2008) Radionuclide tracing of water masses and processes in the water column and sediment in the Algerian Basin. J Environ Radioact 99(8):1224–1232

Olsen CT, Larsen IL, Cutshall NH, Donoghue JF, Bricker OP, Simpson HJ (1981) Reactor released radionuclides in Susquehanna River sediments. Nat 294:242–245

Orlandini KA, Bowling JW, Pinder JE III, Penrose WR (2003) ^{90}Y-^{90}Sr disequilibrium in surface waters: investigating short-term particle dynamics by using a novel isotope pair. Earth Planet Sci Lett 207:141–150

Paatero J, Saxen R, Buyukay M, Outola L (2010) Overview of strontium-89,90 deposition measurements in Finland 1963–2005. J Environ Radioact 101:309–316

Papucci C, Charmasson S, Delfanti R, Gasco C, Mitchell P, Sanchez-Cabeza JA (1996) Time evolution and levels of man-made radioactivity in the Mediterranean Sea. In: Guéguéniat P, Germain P, Métivier H (eds) Radionuclides in the oceans. Inputs and inventories. Les Edition de Physique. Institut de Protection et de Surete Nuclaire, Les Ulis cedex A, pp 177–197

Paytan A, Averyt K, Faul K, Gray E, Thomas E (2007) Barite accumulation, ocean productivity, and Sr/Ba in barite across the Paleocene-Eocene thermal maximum. Geol 35: 1139–1142

Peng T-H, Key RM, Ostlund HG (1998) Temporal variations of bomb radiocarbon inventory in the Pacific Ocean. Mar Chem 60:3–13

Pentreath RJ, Harvey BR, Lovett M (1986) Speciation of fission and activation products in the environment. In: Bulman RA, Cooper JR (eds) Chemical speciation of transuranium nuclides discharged into the marine environment. Elsevier, London, pp 312–325

Periáñez R (2005) Modeling the dispersion of radionuclides by a river plume: application to the Rhone River. Cont Shelf Res 25:1583–1603

Perkins RW, Thomas CW (1980) Worldwide fallout. In: Hanson WC (ed) Transuranic elements in the environment US DOE/TIC-22800. Office of Health and Environmental Research, Washington DC, pp 53–82

Piner KR, Wallace JR, Hamel OS, Mikus R (2006) Evaluation of ageing accuracy of bocaccio (*Sebastes paucispinis*) rockfish using bomb radiocarbon. Fish Res 77:200–206

Povinec PP, Aarkrog A, Buesseler KO, Delfanti R, Hirose K, Hong GH, Ito T, Livingston HD, Nies H, Noshkin VE, Shima S, Togawa O (2005) ^{90}Sr, ^{137}Cs and ^{239,240}Pu concentration surface water time series in the Pacific and Indian Oceans – WOMARS results. J Environ Radioact 81:63–87

Povinec PP, Lee SH, Liong Wee Kwong L, Oregioni B, Jull AJT, Kieser WE, Morgenstern U, Top Z (2010) Top Z (2010) Tritium, radiocarbon, ^{90}Sr and ^{129}I in the Pacific and Indian Oceans. Nucl Instrum Methods Phys Res B 268:1214–1218

Povinec PP, Livingston HD, Shima S, Aoyama M, Gastaud J, Goroncy I, Hirose K, Hyunh-Ngoc L, Ikeuchi Y, Ito T, La Rosa J, Kwong LLW, Lee SH, Moriya H, Mulsow S, Oregioni B, Pettersson H, Togawa O (2003) IAEA'97 expedition to the NW Pacific Ocean – results of oceanographic and radionuclide investigations of the water column. Deep-Sea Res II 50:2607–2637

Raisbeck GM, Yiou F (1999) ^{129}I in the oceans: origins and applications. Sci Total Environ 237(238):31–41

Roether W, Beitzel V, Sultenfu J, Putzka A (1999) The eastern Mediterranean tritium distribution in 1987. J Mar Syst 20:49–61

Roy-Barman M (2009) Modelling the effect of boundary scavenging of thorium and protactinium profiles in the ocean. Biogeosci 6:3091–3107

Santschi PH, Presley BJ, Wade TL, Garcia-Romero B, Baskaran M (2001) Historical contamination of PAHs, PCBs, DDTs, and heavy metals in Mississippi River Delta, Galveston Bay and Tampa Bay sediment cores. Mar Environ Res 52:51–79

Schink DR, Santschi PH, Corapcioglu O, Fehn U (1995) Prospects for "iodine-129 dating" of marine organic matter using AMS. Nucl Instrum Methods Phys Res B 99:524–527

Schlosser P, Bonisch G, Kromer B, Loosli HH, Buhler R, Bayer R, Bonani G, Koltermann P (1995) Mid-1980s distribution of tritium, ^{3}He, ^{14}C and ^{39}Ar in the Greenland/Norwegian Seas and the Nansen Basin of the Arctic Ocean. Prog Oceanogr 35:1–28

Sholkovitz ER (1983) The geochemistry of plutonium in fresh and marine water environments. Earth Sci Rev 19:95–161

Shlokovitz ER, Mann DR (1987) ^{239,240}Pu in estuarine and shelf waters of the north-eastern United States. Estuarine Coast Shelf Sci 25:413–434

Smith JN, Ellis KM, Jones EP (1990) Caesium-137 transport into the Arctic Ocean through Fram Strait. J Geophys Res 95 (C2):1693–1701

Smith JN, Elis KM, Naes K, Dahle S, Matishov D (1995) Sedimentation and mixing rates of radionuclides in Barents Sea sediments off Novaya Zemlya. Deep-Sea Res II 42: 1471–1493

Smethie WM Jr, Ostlund HG, Loosli HH (1986) Ventilation of the deep Greenland and Norwegian seas: evidence from krypton-85, tritium, carbon-14 and argon-39. Deep-Sea Res 33:675–703

Spencer DW, Bacon MP, Brewer PG (1981) Models of the distribution of ^{210}Pb in a section across the north Equatorial Atalntic Ocean. J Mar Res 39:119–138

Stokozov NA, Buesseler KO (1999) Mixing model for the northwest Black Sea using ^{90}Sr and salinity as tracers. J Environ Radioact 43:173–186

Tkalin AV, Chaykovskaya EL (2000) Anthropogenic radionuclides in Peter the Great Bay. J Environ Radioact 51:229–238

Topcuoğlu S, Güngör N, Kirbaşaoğlu C (2002) Distribution coefficients (K_d) and desorption rates of ^{137}Cs and ^{241}Am in Black Sea sediments. Chemos 49:1367–1373

UNSCEAR (2000) United Nations Scientific Committee on the Effects of Atomic Radiation (UNSCEAR) Report to the

general assembly with scientific annexes. Annex C: exposures from man-made sources of radiation. http://www.unscear.org. Accessed April 2010

Vakulovsky S (1987) Determination of distribution processes, transport routes and transport times in the North Sea and the northern North Atlantic using artificial radionuclides as tracers. In: Guary JC, Guegueniat P, Pentreath RJ (eds) Radionuclides: a tool for oceanography. Elsevier Applied Science, London, pp 271–280

Vakulovsky S (2001) Radiation monitoring in Russia at the turn of the millennium. J Eniron Radioact 55:219–220

Warneke T, Croudace IW, Warwick PE, Taylor RN (2002) A new ground-level fallout record of uranium and plutonium isotopes for northern temperate latitudes. Earth Planet Sci Lett 203:1047–1057

Weimer W, Langford JC (1978) Iron-55 and stable iron in oceanic aerosols: forms and availability. Atmos Environ 12:1201–1205

Winger K, Feichter J, Kalinowski MB, Sartorius H, Schlosser C (2005) A new compilation of the atmospheric ^{85}krypton inventories from 1945 to 2000 and its evaluation in a global transport model. J Environ Radioact 80:183–215

Wong KM, Jokela TA, Eagle RJ, Brunk JL, Noshkin VE (1992) Radionuclide concentrations, fluxes, and residence times at Santa Monica and San Pedro Basins. Prog Oceanogr 30: 353–391

Yamada M, Wang Z-L, Zhen J (2006) The extremely high ^{137}Cs inventory in the Sulu Sea: a possible mechanism. J Environ Radioact 90:163–171

Yim MS, Caron F (2006) Life cycle and management of carbon-14 from nuclear power generation. Prog Nucl Energy 48:2–36

Yiou F, Raisbeck GM, Christensen GC, Holm E (2002) ^{129}I/^{127}I, ^{129}I/^{137}Cs and ^{129}I/^{99}Tc in the Norwegian coastal current from 1980 to 1988. J Environ Radioact 60:61–71

Yoshida S, Muramatsu Y (2003) Determination of U and Pu isotopes in environmental samples by inductively coupled plasma mass spectrometry. http://www.nirs.go.jp/report/nene/h13/05/85.htm. Accessed April 2010